

Meiotic DNA break formation requires the unsynapsed chromosome axis-binding protein IHO1 (CCDC36) in mice

Marcello Stanzione¹, Marek Baumann^{1,7}, Frantzeskos Papanikos¹, Ihsan Dereli¹, Julian Lange², Angelique Ramlal^{1,7}, Daniel Tränkner¹, Hiroki Shibuya^{3,7}, Bernard de Massy⁴, Yoshinori Watanabe³, Maria Jasinska⁵, Scott Keeney^{2,6} and Attila Tóth^{1,8}

DNA double-strand breaks (DSBs) are induced by SPO11 during meiosis to initiate recombination-mediated pairing and synapsis of homologous chromosomes. Germline genome integrity requires spatiotemporal control of DSB formation, which involves the proteinaceous chromosome axis along the core of each meiotic chromosome. In particular, a component of unsynapsed axes, HORMAD1, promotes DSB formation in unsynapsed regions where DSB formation must occur to ensure completion of synapsis. Despite its importance, the underlying mechanism has remained elusive. We identify CCDC36 as a direct interactor of HORMAD1 (IHO1) that is essential for DSB formation. Underpinning this function, IHO1 and conserved SPO11-auxiliary proteins MEI4 and REC114 assemble chromatin-bound recombinosomes that are predicted activators of DSB formation. HORMAD1 is needed for robust recruitment of IHO1 to unsynapsed axes and efficient formation and/or stabilization of these recombinosomes. Thus, we propose that HORMAD1–IHO1 interaction provides a mechanism for the selective promotion of DSB formation along unsynapsed chromosome axes.

Generation of haploid gametes requires segregation of homologous chromosomes (homologues) during the first meiotic division. In most taxa including mammals, each pair of homologues must engage and become physically linked via at least one crossover during the first prophase to achieve high-fidelity segregation^{1,2}. Inter-homologue crossovers are formed by homologous recombination, which initiates with SPO11 transesterase-mediated induction of multiple DSBs in early prophase^{3,4}. Homology search initiated by multiple DSBs on each chromosome results in close juxtaposition of homologues along their lengths. The number of DSBs is tightly controlled: having too many may yield genotoxic effects, while too few would not ensure high-fidelity homologue pairing. Feedback control from homologue pairing to DSB formation and repair may help meet these requirements^{5–8}.

Spatiotemporal control of recombination relies on two meiosis-specific chromatin structures: the chromosome axis and the synaptonemal complex (SC). The axis is a rod-like proteinaceous

structure that forms early in meiosis along the cohesin core of each sister chromatid pair. The SC is a structure that forms when homologue axes pair and become closely linked along their lengths in a zipper-like fashion by transverse filament proteins^{7,9}. Meiosis-specific HORMA-domain proteins are axis components that mediate key functions in control of DSB formation and repair and/or in the quality control of recombination in diverse taxa^{7,9,10}. In mammals, the HORMA-domain protein HORMAD1 preferentially associates with unsynapsed axes^{5,11} and is thought to have three main functions^{12–15}. First, it ensures availability of sufficient DSBs for homology search by promoting DSB formation, and possibly by inhibiting premature DSB repair or inappropriate recombination between sister chromatids. Second, HORMAD1 supports SC formation. Third, HORMAD1 sets up checkpoints that prevent progression of meiocytes beyond prophase unless homologues are synapsed. SC formation is proposed to inhibit HORMAD1 functions and promote the depletion of

¹Institute of Physiological Chemistry, Faculty of Medicine at the TU Dresden, Fetscherstraße 74, 01307 Dresden, Germany. ²Molecular Biology Program, Memorial Sloan Kettering Cancer Center, New York, New York 10065, USA. ³Institute of Molecular and Cellular Biosciences, University of Tokyo, Yayoi 1-1-1, Tokyo 113-0032, Japan. ⁴Institute of Human Genetics, UPR 1142, CNRS, University of Montpellier, 141, rue de la Cardonille, 34396 Montpellier, France. ⁵Developmental Biology Program, Memorial Sloan Kettering Cancer Center, New York, New York 10065, USA. ⁶Howard Hughes Medical Institute, Memorial Sloan Kettering Cancer Center, New York, New York 10065, USA. ⁷Present addresses: GlaxoSmithKline Biologicals NL der SmithKline Beecham Pharma GmbH & Co. KG, Zirkusstrasse 40, 01069 Dresden, Germany (M.B.); Department of Human Genetics, Radboud University Medical Center, Geert Goopteplein 10, 6525 GA Nijmegen, The Netherlands (A.R.); Department of Chemistry and Molecular Biology, University of Gothenburg, 40530 Gothenburg, Sweden (H.S.). ⁸Correspondence should be addressed to A.T. (e-mail: attila.toth@mailbox.tu-dresden.de)

Received 18 March 2016; accepted 6 September 2016; published online 10 October 2016; DOI: 10.1038/ncb3417

HORMAD1 from axes^{5,12}. This is one likely, but not exclusive, mechanism by which SC formation may also downregulate DSB formation and enable progression of meiocytes beyond prophase once homologues are successfully paired^{5,7,12,16}. In this model, SC formation limits DSB numbers by restricting DSB formation to unsynapsed axes, precisely where DSBs are still needed to promote homologue engagement and SC formation^{5,7}. Indeed, the SC appears to downregulate DSB formation both in budding yeast and mice^{6,8}. A major goal is to identify the mechanisms that govern relationships between DSB formation and the chromosome axis.

The prevailing molecular model of meiotic DSB formation is based mainly on studies of yeast. Chromatin is arranged in loops emanating from the chromosome axis, and DSBs form preferentially in loop-forming DNA as opposed to axis-bound DNA^{17,18}. However, it is thought that DSBs are introduced only after ‘loop DNAs’ have been recruited to axes, because DSB-promoting protein complexes—recombinosomes—assemble only along axes^{17,18}. In yeasts, complexes containing the conserved Mei4 and Rec114 proteins and a third coiled-coil-containing protein (Mer2 and Rec15 in budding and fission yeasts, respectively) are thought to link Spo11 activity to axes^{9,18–22}. MEI4 and REC114 are also present in mammals²³. Mouse MEI4 is indispensable for DSB formation, and it interacts with REC114 and forms foci along unsynapsed chromosome axes²³. These foci are thought to represent DSB-promoting recombinosomes because focus formation along axes correlates with DSB formation^{16,23}. HORMAD1 that is associated with unsynapsed axes appears to be important for the function of these recombinosomes, as HORMAD1 is needed for efficient DSB formation^{12–14} and high MEI4 focus numbers¹⁶. However, pivotal questions remain unanswered. It is poorly understood what the composition and importance of axis-associated putative DSB-promoting recombinosomes are, and what mechanism targets their assembly and DSB formation to HORMAD1-rich unsynapsed axes.

RESULTS

IHO1, a component of unsynapsed axes

To gain insights into axis functions, we screened for HORMAD1-interacting proteins by yeast two-hybrid assay and identified CCDC36, which we named interactor of HORMAD1-1 (IHO1). Both mouse and human protein pairs interact. IHO1 is a coiled-coil-domain-containing protein without other recognizable domains or annotated functions and is conserved in vertebrates. Mouse ENCODE data^{24,25} and PCR with reverse transcription (Supplementary Fig. 1a) showed testis enrichment of *Iho1* transcripts, and anti-IHO1 antibodies preferentially stained spermatocytes in testis sections (Fig. 1a). HORMAD1 co-precipitated with IHO1 from testis extracts (Fig. 1b), and immunostaining of spread meiocytes revealed that IHO1, like HORMAD1, associates with chromatin during prophase (Fig. 1c,d and Supplementary Fig. 1b–d). IHO1 and HORMAD1 foci appeared on chromatin during preleptotene, when pre-meiotic replication occurs and axes have not yet developed (Fig. 1d and Supplementary Fig. 1b–d). In leptotene, IHO1 displayed increasing intensity along developing HORMAD1-rich axes. In zygotene, when axes elongate and synapsis begins, IHO1 remained associated with unsynapsed axes but disappeared from synapsed axes (Fig. 1c,d and Supplementary Fig. 1c,d). Although IHO1 and HORMAD1 largely co-localized, IHO1

staining was more discontinuous and more completely depleted from synapsed regions (Fig. 1c,d).

IHO1 localization diverged in the two sexes beyond zygotene. In spermatocytes, synapsis between the largely non-homologous X and Y chromosomes is mostly constrained to their short pseudoautosomal regions (PARs). At the zygotene-to-pachytene transition, high IHO1 and HORMAD1 levels remained on unsynapsed sex chromosome axes but also on PARs (Supplementary Fig. 2)⁵. However, by early pachytene IHO1 disappeared from both the synapsed and unsynapsed regions of sex chromosomes (Supplementary Fig. 2), contrasting persistent HORMAD1 association with unsynapsed axes in pachytene^{5,11}. Curiously, IHO1 re-accumulated on unsynapsed axes of sex chromosomes in mid-late pachytene and on desynapsing autosome axes in diplotene, but disappeared from chromatin concomitant with axis disassembly after diplotene (Supplementary Figs 1c and 2). In oocytes, IHO1 disappeared from axes after all chromosomes synapsed and was undetectable on chromatin beyond zygotene (Supplementary Fig. 1d). Ovarian IHO1 levels also dramatically decreased as oocytes progressed to late prophase (Supplementary Fig. 1e).

The preferential enrichment of both IHO1 and HORMAD1 on unsynapsed axes (albeit with some differences in localization) supports the idea that they interact *in vivo*. Concordantly, HORMAD1 was required for robust IHO1 accumulation on chromatin and unsynapsed axes (Fig. 1d) and for high IHO1 levels in chromatin-rich fractions of testis extracts (Fig. 1e), suggesting that HORMAD1 recruits IHO1 to unsynapsed axes. To test the hypothesis that IHO1 may mediate some or all HORMAD1-dependent axis functions, we disrupted the *Iho1* gene in mice (Supplementary Fig. 3).

Iho1^{−/−} mice are defective in homologous synapsis

Iho1^{−/−} mice were viable without obvious somatic defects, but both sexes were infertile (96 breeding-weeks, 2 males and 4 females). Oocytes were depleted in six-week-old *Iho1*^{−/−} females, and spermatocytes in males underwent apoptosis at a stage equivalent to wild-type mid-pachytene (Supplementary Fig. 4), suggestive of meiotic recombination defects^{26–29}. Cohesin cores, chromosome axes, and HORMAD1 recruitment to unsynapsed axes appeared normal, but axis alignment and SC formation were severely defective (Fig. 2b and Supplementary Fig. 5). Complete synapsis was never observed, but incomplete SCs were detected in meiocytes equivalent to late-zygotene and pachytene as judged by the presence of fully formed axes ($n > 500$ cells, Fig. 2b). SC was observed between axes of unequal length and between multiple partners in most if not all meiocytes displaying extensive synapsis ($n > 100$ cells, Fig. 2b and Supplementary Fig. 5h); thus, SC often forms between non-homologous chromosomes. This contrasts *Hormad1*^{−/−} meiocytes, where reduced DSB numbers yield incomplete SC formation that nonetheless occurs mostly between homologues^{12,13}.

Aberrant SC in *Iho1*^{−/−} meiocytes may be explained by defective homologue pairing. Alternatively, IHO1 may function in a manner independent of pairing, similar to HORMAD1. The latter is required for non-homologous synapsis that occurs extensively in the DSB-deficient *Spo11*^{−/−} background, where homologue pairing fails^{12,13}. To distinguish between these possibilities, we compared effects of *Iho1* and *Hormad1* mutations on SC formation in the *Spo11*^{−/−} background (Fig. 2). *Iho1*^{−/−}*Spo11*^{−/−} and *Iho1*^{−/−} spermatocytes were equally proficient as *Spo11*^{−/−} in forming non-homologous SC, whereas

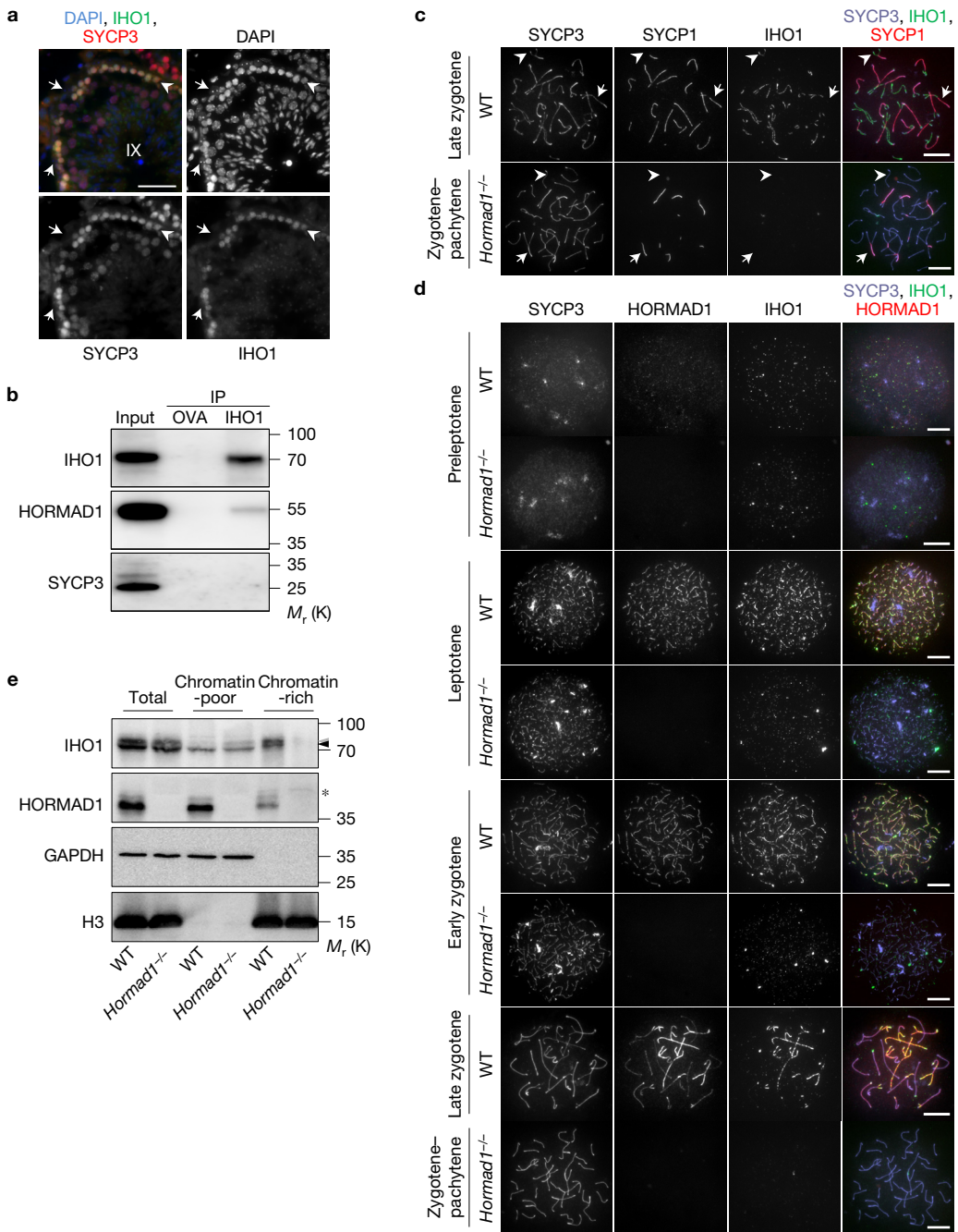


Figure 1 IHO1, interactor of HORMAD1, localizes to unsynapsed axes. **(a)** SYCP3 (meiotic axis marker) and IHO1 were detected by immunofluorescence, and DNA by DAPI, on wild-type testis cryosections. A stage IX tubule is shown. IHO1 signal is strong only in meiotic leptotene cells (arrowhead) and is absent from non-meiotic Sertoli cells (arrows). Scale bar, 50 µm. **(b)** Solubilized chromatin fractions of wild-type testes were subjected to immunoprecipitation by anti-ovalbumin (OVA) or anti-IHO1 (IHO1) antibody. Input (equivalent to 5% of immunoprecipitation samples) and immunoprecipitated (IP) samples were analysed by immunoblotting with anti-IHO1, anti-HORMAD1 and anti-SYCP3 antibodies. HORMAD1 but not SYCP3 co-precipitates with IHO1, indicating that IHO1–HORMAD1 co-precipitation is not mediated by the chromosome axis. Anti-OVA immunoprecipitation served as a negative control. **(c,d)** IHO1, SYCP3, and either SYCP1 (synaptonemal complex transverse filament) **(c)** or HORMAD1 **(d)** were detected by immunofluorescence on nuclear surface spreads of wild-type and Hormad1^{-/-} spermatocytes. Equal exposure images are shown. IHO1 appears

on chromatin in preleptotene and preferentially accumulates on unsynapsed chromosome axes in wild-type (WT) cells at later stages. IHO1 levels are much lower on chromatin and unsynapsed axes in Hormad1^{-/-} spermatocytes at corresponding stages. Stages corresponding to wild-type late zygotene and early pachytene cannot be distinguished in Hormad1^{-/-} due to defective SC formation; hence we refer to this stage as 'zygotene–pachytene'. Arrows and arrowheads in **c** indicate synapsed and unsynapsed axes, respectively. Scale bars in **c** and **d**, 10 µm. **(e)** Total, Triton X-100-soluble (chromatin-poor) and -insoluble (chromatin-rich) extracts were prepared from testes of 13 days postpartum wild-type and Hormad1^{-/-} littermates and analysed by immunoblotting. IHO1 levels in the chromatin-rich Triton X-100-insoluble fraction are much lower in Hormad1^{-/-} than in wild type. Black and grey arrowheads mark IHO1-specific bands. H3, histone H3. Unprocessed original scans of the gels in **b** and **e** are shown in Supplementary Fig. 8.

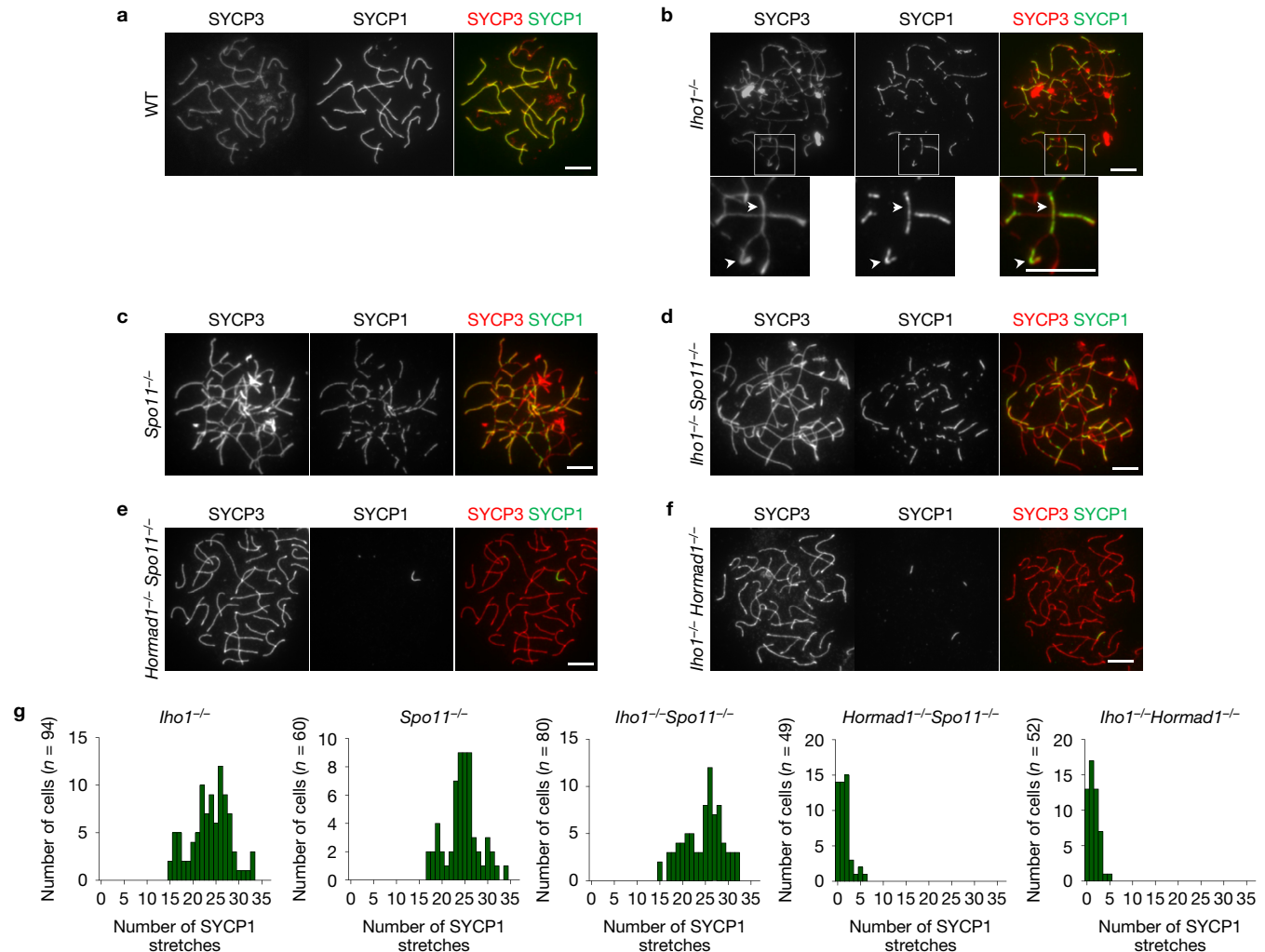


Figure 2 SC formation and alignment of chromosome axes is defective in *Iho1*^{-/-} spermatocytes. **(a–f)** SYCP3 (axis marker) and SYCP1 (SC marker) were detected by immunofluorescence on nuclear surface spreads of wild-type (WT) pachytene **(a)** and mutant zygotene–pachytene spermatocytes of the indicated genotypes. Scale bars, 10 µm. **(b)** Homologous chromosomes are not aligned in the presented image of an *Iho1*^{-/-} spermatocyte; however, SCs form between apparently non-homologous chromosomes, creating a meshwork of interconnected axes. The insets show an enlarged view. Arrowheads mark sites where a chromosome axis is engaged in synapsis with two different partners. This phenotype resembles those of *Spo11*^{-/-} **(c)** and *Iho1*^{-/-} *Spo11*^{-/-} **(d)** spermatocytes, in which DNA strand invasion and homologue pairing are defective due to a lack of DSBs. SYCP1 stretches are much shorter **(e,f)** and less numerous in *Hormad1*^{-/-} *Spo11*^{-/-} **(e)** and *Iho1*^{-/-} *Hormad1*^{-/-} **(f)** spermatocytes than in *Iho1*^{-/-} **(b)**, *Spo11*^{-/-} **(c)** or *Iho1*^{-/-}

Spo11^{-/-} **(d)** spermatocytes. **(g)** The frequency distributions of SYCP1 stretch numbers in zygotene–pachytene spermatocytes with fully condensed axes. *n* shows analysed spermatocyte number from two (*Hormad1*^{-/-} *Spo11*^{-/-} and *Iho1*^{-/-} *Hormad1*^{-/-}) or three (*Iho1*^{-/-}, *Spo11*^{-/-} and *Iho1*^{-/-} *Spo11*^{-/-}) pooled experimental repeats. Numbers of SYCP1 stretches were not significantly different in *Iho1*^{-/-}, *Spo11*^{-/-} and *Iho1*^{-/-} *Spo11*^{-/-} (*Iho1*^{-/-} versus *Spo11*^{-/-}, $P=0.3668$; *Iho1*^{-/-} versus *Iho1*^{-/-} *Spo11*^{-/-}, $P=0.1596$; *Spo11*^{-/-} versus *Iho1*^{-/-} *Spo11*^{-/-}, $P=0.5197$; Mann–Whitney test), but SYCP1 stretch numbers were higher in these three genotypes than in *Iho1*^{-/-} *Hormad1*^{-/-} and *Hormad1*^{-/-} *Spo11*^{-/-} spermatocytes ($P<2.20\times10^{-16}$ for all comparisons, Mann–Whitney test). SC formation was not significantly different in *Iho1*^{-/-} *Hormad1*^{-/-} and *Hormad1*^{-/-} *Spo11*^{-/-} spermatocytes ($P=0.9162$, Mann–Whitney test). Primary source data of graphs are available in Supplementary Table 2.

Hormad1 deficiency largely abolished SC in both the *Spo11*^{-/-} and *Iho1*^{-/-} backgrounds. Thus, whilst HORMAD1 has a function allowing homologue-pairing-independent SC in *Spo11*^{-/-}, IHO1 does not.

IHO1 is required for DSB formation

The indistinguishable non-homologous SC formation phenotypes in *Spo11*^{-/-} and *Iho1*^{-/-} meiocytes could be explained if IHO1, like SPO11, is required for DSB formation. Consistent with this hypothesis, *Iho1*^{-/-} spermatocytes formed few or no foci of recombination proteins that mark DSB ends, a number comparable

to that in *Spo11*^{-/-}, but much lower than in *Hormad1*^{-/-} (Fig. 3a–f). Likewise, phospho-histone H2AX (γ H2AX), a marker of the ATM/ATR-dependent DNA damage response, was virtually absent from chromatin in leptotene and early zygotene in both *Spo11*^{-/-} and *Iho1*^{-/-} spermatocytes, contrasting the reduced but still present staining in *Hormad1*^{-/-} (Supplementary Fig. 6). Initial DSB processing generates SPO11-oligonucleotide complexes whose levels in testis extracts indicate DSB levels³⁰. SPO11-oligonucleotide complexes were absent from both *Spo11*^{-/-} and *Iho1*^{-/-} testes (*n*=3 mice per genotype) (Fig. 3g,h), whereas they were detectable in

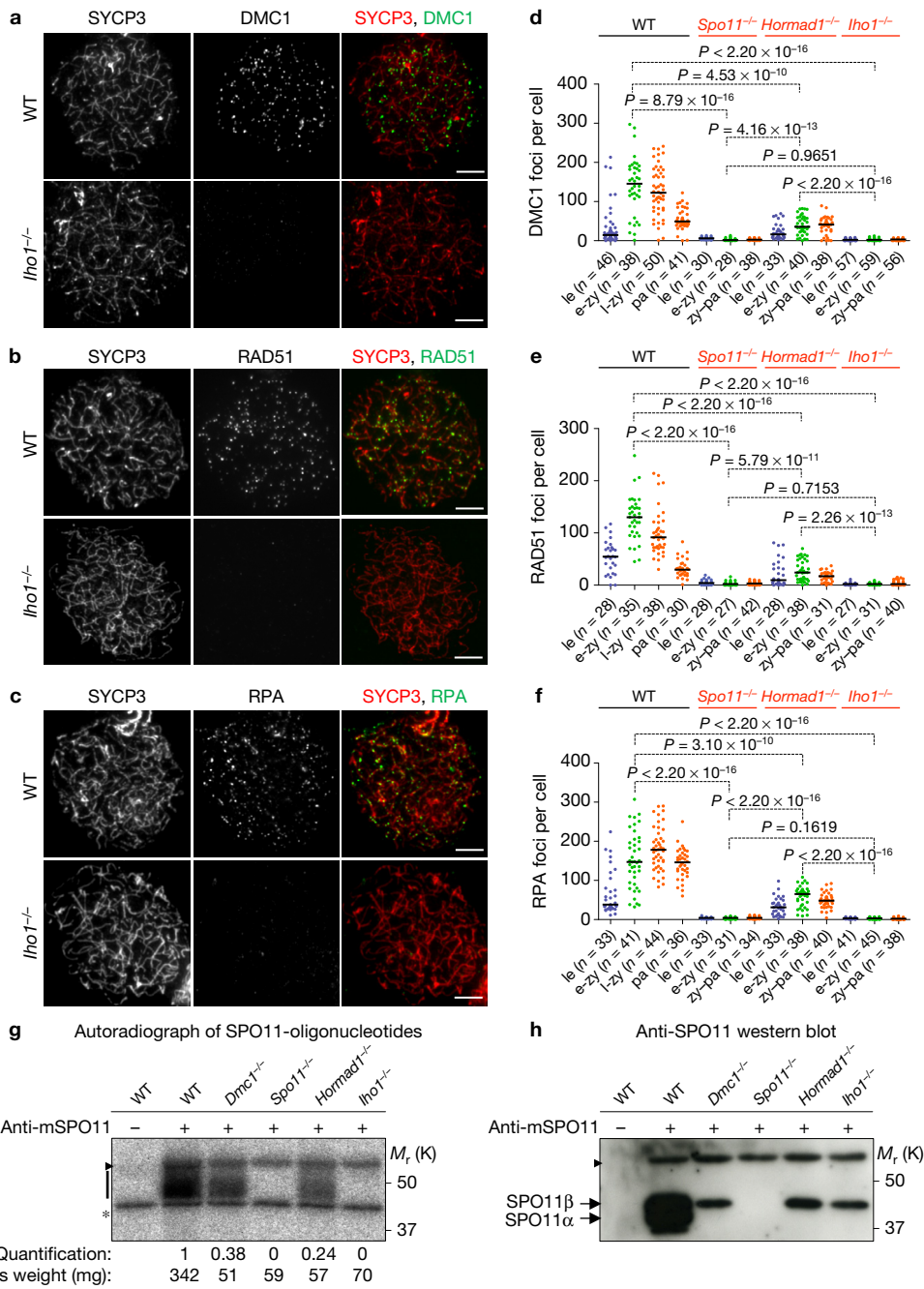


Figure 3 Recombination foci and SPO11-oligonucleotides are effectively absent from *Iho1^{-/-}* spermatocytes and testes, respectively. (a–c) SYCP3 (axis marker) and DMC1 (a), RAD51 (b) or RPA (c) (markers of recombination/single-stranded DSB ends) were detected on nuclear surface spreads of wild-type (WT) and *Iho1^{-/-}* zygotene spermatocytes. Scale bars, 10 μ m. (d–f) Numbers of DMC1 (d), RAD51 (e) and RPA (f) foci during leptotene (le) and early zygotene (e-zy) in wild type, *Spo11^{-/-}*, *Hormad1^{-/-}* and *Iho1^{-/-}*; late zygotene (l-zy) and pachytene (pa) in wild type; and zygotene–pachytene (zy–pa) in *Spo11^{-/-}*, *Hormad1^{-/-}* and *Iho1^{-/-}*. Median focus numbers are marked; n shows analysed spermatocyte number from three (RAD51 and RPA) or four (DMC1) pooled experiments. P values were calculated by Mann–Whitney test. DMC1, RAD51 and RPA focus numbers in *Hormad1^{-/-}* were on average 29%, 22% and 39% of wild type, respectively, during the comparable early-zygotene stage. Virtually no recombination foci were detected in *Iho1^{-/-}* (on average 2%, 2% and 2% of wild-type DMC1, RAD51 and RPA, respectively) and *Spo11^{-/-}* (on average 2%, 2% and 2% of wild-type DMC1, RAD51, respectively). (g,h) SPO11-oligonucleotide

complexes (g) and SPO11 protein (h) were detected in adult testis extracts. *Dmc1^{-/-}* testes were used to control for altered cellularity in mutant testes; *Dmc1^{-/-}*, *Spo11^{-/-}*, *Hormad1^{-/-}* and *Iho1^{-/-}* testes are characterized by apoptosis of mid-pachytene-equivalent spermatocytes in tubules at stage IV of the seminiferous epithelial cycle. One representative of three experiments is shown. (g) SPO11-oligonucleotide complexes were immunoprecipitated and radioactively labelled. The bar marks SPO11-specific signals, the asterisk indicates nonspecific labelling of contaminants, and the arrowhead marks the immunoglobulin heavy chain. Quantified levels of radioactive signals were background-corrected and normalized to wild type. (h) Blots from g were probed with anti-SPO11 antibody. Two alternative forms of SPO11 (α and β) protein were present in wild type^{30,47,48}. Only SPO11 β , the form that is expressed in early meiosis, was detected in *Dmc1^{-/-}*, *Hormad1^{-/-}* and *Iho1^{-/-}* mutants. Unprocessed original scans of gels are shown in Supplementary Fig. 8. Primary source data of recombination focus counts and SPO11-oligonucleotide quantifications are shown in Supplementary Table 2.

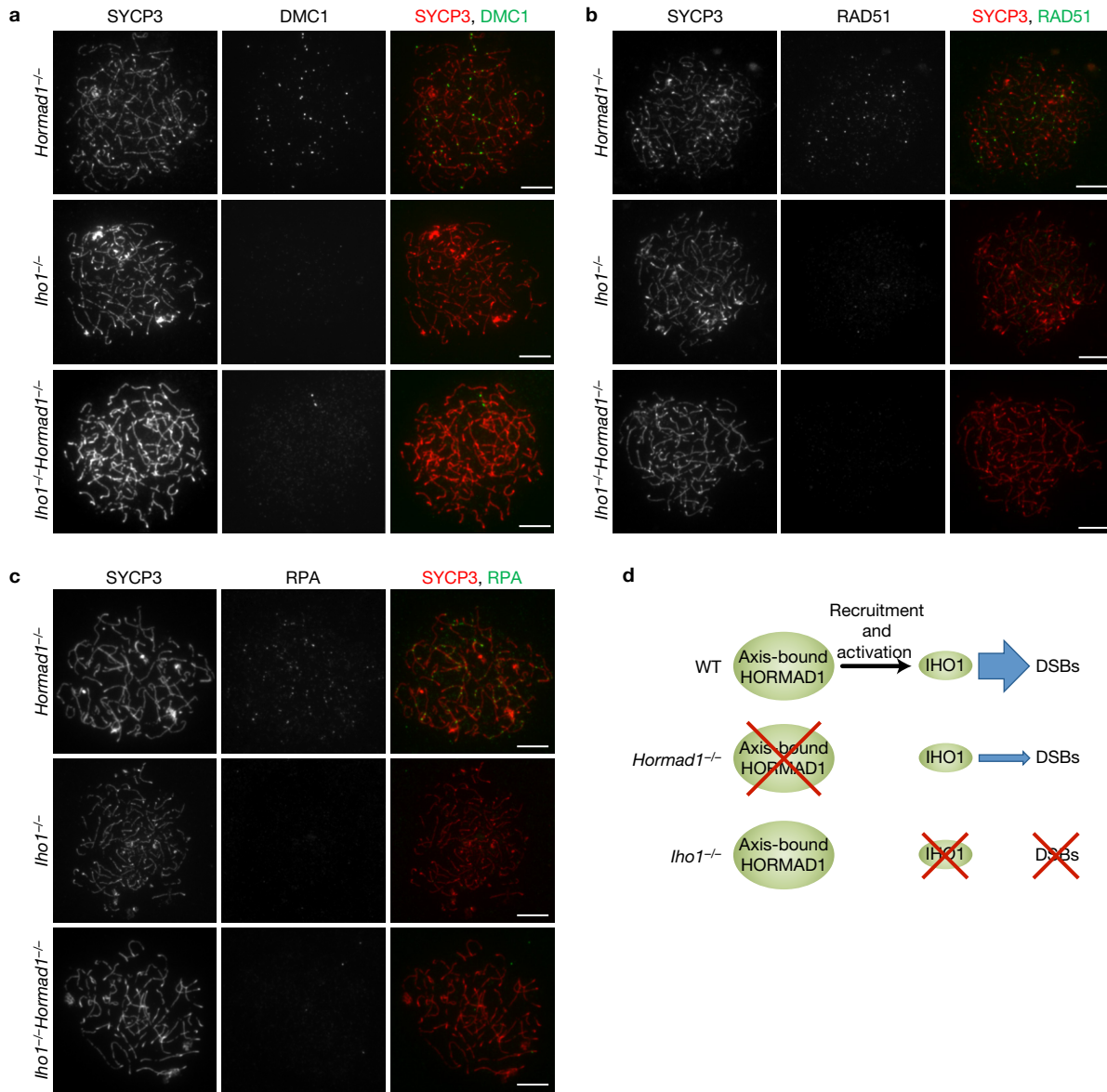


Figure 4 IHO1 has HORMAD1-independent DSB-formation-promoting activity. (a–c) SYCP3 and either DMC1 (a), RAD51 (b) or RPA (c) recombination markers were detected by immunofluorescence on nuclear surface spreads of *Hormad1*^{-/-}, *Iho1*^{-/-} and *Iho1*^{-/-}*Hormad1*^{-/-} zygote spermatocytes. Whereas foci of all three marker proteins were readily detected in *Hormad1*^{-/-}, they were essentially absent from *Iho1*^{-/-} and *Iho1*^{-/-}*Hormad1*^{-/-}.

Hormad1^{-/-} testes at reduced levels compared with wild type (median 4.3-fold reduction, $P=0.00027$, $n=7$, one-sample t -test) or *Dmc1*^{-/-} (median 2.4-fold reduction, $P=0.0068$, $n=7$, one-sample t -test based on current and published¹² results). (*Dmc1*^{-/-} mice provide DSB-formation-proficient controls for altered testis size and cellularity of *Spo11*^{-/-}, *Hormad1*^{-/-} and *Iho1*^{-/-} mutants, because pachytene-equivalent spermatocytes are eliminated in all of these mutants at stage IV of the epithelial cycle of seminiferous tubules^{12–14,27,31,32}; Supplementary Fig. 4a.) These observations strongly suggest that programmed meiotic DSB formation is abolished in *Iho1*^{-/-} mice.

Similar to *Iho1*^{-/-} single mutants, *Iho1*^{-/-}*Hormad1*^{-/-} double-mutant spermatocytes had many fewer RAD51, DMC1 or RPA foci

Hormad1^{-/-} spermatocytes ($n>200$ cells examined for each staining). Scale bars, 10 μ m. (d) Model depicting the likely functional interplay between IHO1 and HORMAD1 in DSB formation. The blue arrows represent promotion of DSB formation by IHO1 proportionally to the thickness of the arrow. The black arrow represents HORMAD1-mediated recruitment of IHO1 to axes and promotion of IHO1 activity.

than *Hormad1*^{-/-} spermatocytes (Fig. 4a–c). Thus, *Iho1* is epistatic to *Hormad1* in DSB formation, indicating that IHO1 is able to promote DSB formation even in the absence of HORMAD1. HORMAD1 may enhance this basal HORMAD1-independent IHO1 activity and IHO1 association with axes, thereby ensuring efficient DSB formation.

IHO1 is dispensable for HORMAD1-mediated meiotic prophase quality control

HORMAD1 and its parologue HORMAD2 have crucial functions in quality control mechanisms that eliminate meiocytes in response to inappropriate synapsis^{12,13,33,34}. HORMAD1/2 promote recruitment of ATR activity to unsynapsed regions, resulting in H2AX

phosphorylation and meiotic silencing of unsynapsed chromatin (MSUC)^{12,13,33–36}. In pachytene spermatocytes, MSUC forms the sex body, the silenced chromatin that encompasses unsynapsed portions of the sex chromosomes and turns off genes whose expression is toxic at this stage^{26,35,37–39}. Both extensive autosomal asynapsis and impaired HORMAD1 function cause spermatocyte elimination from failed sex chromosome silencing^{12–14,26,29}. Autosomal asynapsis lowers ATR activity on sex chromosomes by redistributing ATR to unsynapsed autosomes²⁹, whereas HORMAD1 deficiency impairs recruitment of ATR activity to all unsynapsed axes, including sex chromosomes^{12–14}.

To test whether IHO1 has a role similar to HORMAD1, we examined recruitment of ATR and the ATR activator BRCA1 as well as ATR activity (γ H2AX accumulation) on unsynapsed chromatin. To control for the absence of DSBs in *Iho1*^{−/−}, we compared it with *Spo11*^{−/−} in addition to wild type. HORMAD1, ATR and BRCA1 were all recruited to unsynapsed axes and/or chromatin similarly in *Spo11*^{−/−} and *Iho1*^{−/−} spermatocytes, and recruitment of ATR and BRCA1 required HORMAD1 in both backgrounds (Fig. 5a–d). Correspondingly, high fractions of *Iho1*^{−/−} and *Spo11*^{−/−} spermatocytes accumulated γ H2AX in ‘pseudo-sex bodies’, which form around undefined subsets of unsynapsed axes due to spurious HORMAD1-dependent ATR signalling in DSB-defective mutants^{12,13,27,40}. Importantly, efficient pseudo-sex-body formation depended on HORMAD1 in both backgrounds (Fig. 5a,e). Thus, IHO1 is not involved in HORMAD1-mediated surveillance of asynapsis or ATR activation in unsynapsed regions.

This conclusion is supported by the near absence of oocytes in 6-week-old *Iho1*^{−/−} mice (Supplementary Fig. 4b), which shows that IHO1, unlike HORMAD1, is dispensable for elimination of asynaptic oocytes. In females, persistent ATR signalling and/or inappropriate silencing of *ad hoc* sets of essential genes by MSUC (both dependent on HORMAD1) are thought to eliminate asynaptic oocytes during prophase⁴¹.

IHO1 is required for robust MEI4 focus formation on chromatin

Having found that IHO1 is required for DSBs, we asked how IHO1 promotes DSB formation. The budding yeast HORMA-domain protein Hop1 helps recruit Mei4, Rec114 and Mer2 to axes¹⁸ and mouse HORMAD1 is required for normal appearance of MEI4 foci that are presumptive DSB-promoting recombinosomes¹⁶. If IHO1 mediates HORMAD1 function in DSB formation, then IHO1 loss should also affect MEI4 complex assembly. MEI4 levels in testis extracts were comparable but MEI4 foci were 11-fold and 6-fold fewer in *Iho1*^{−/−} leptotene spermatocytes than in wild type or *Hormad1*^{−/−}, respectively (Fig. 6a–c). *Iho1*^{−/−} and *Iho1*^{−/−} *Hormad1*^{−/−} spermatocytes were comparable (Fig. 6a); thus, *Iho1* is epistatic to *Hormad1* in both DSB formation and MEI4 focus formation. MEI4 foci appear more stable in *Spo11*^{−/−} than in wild type²³, raising the possibility that SPO11 not only promotes DSB formation but also directly or indirectly destabilizes DSB-promoting protein complexes. IHO1 deficiency caused fewer MEI4 foci to form in both *Spo11*^{+/−} and *Spo11*^{−/−} backgrounds (Fig. 6d,e), so this defect in MEI4 focus formation is not a consequence of increased sensitivity to a putative recombinosome destabilizing activity of SPO11.

We cannot exclude that HORMAD1 and IHO1 foster DSB formation through distinct mechanisms. It is also possible that

HORMAD1 affects DSB formation indirectly, for example, by altering timing of meiotic events via its checkpoint function, although available data argue against such a role for yeast Hop1 (ref. 42). Nevertheless, our observations suggest that IHO1 and HORMAD1 collaborate in DSB formation. Specifically, IHO1 probably stimulates DSB formation through efficient formation of MEI4-containing recombinosomes, and HORMAD1 probably enhances this function. This hypothesis may explain why *Iho1*^{−/−} spermatocytes do not form any programmed DSBs while *Hormad1*^{−/−} spermatocytes do, albeit fewer than wild type.

Putative chromatin-bound DSB-promoting recombinosomes contain IHO1

We hypothesized that IHO1 might form complexes with MEI4 on chromatin. Supporting this, the majority of MEI4 foci co-localized with IHO1 in preleptotene wild-type cells, that is, when IHO1 forms only foci and when elongated axis structures and DSBs have not yet formed (Fig. 7a,b). Note that only 53% (preleptotene, $n = 17$ cells) and 65% (leptotene, $n = 43$ cells) of foci detected by the anti-MEI4 guinea pig antibody overlapped with foci detected by the anti-MEI4 rabbit antibody (Supplementary Table 2, ‘gpMEI4-rbMEI4-coloc’), suggesting that half to two-thirds of foci detected by the guinea pig antibody represented genuine chromatin-associated MEI4 complexes. (For antibody validation, see Methods.) Given this observation, co-localizing MEI4-IHO1 foci (61% of MEI4 foci) may represent most, if not all, genuine MEI4-containing complexes. MEI4 foci were also preferentially detected along stretches of IHO1 staining that marked forming axes from leptotene onwards (Fig. 7a lower panel, b), indicating that MEI4 and IHO1 probably remain in a complex along axes in later stages. Importantly, the *Hormad1*^{−/−} mutant displayed low-intensity IHO1 foci despite strongly reduced IHO1 levels and failure of IHO1 to spread along unsynapsed axes (Fig. 1d). A large fraction of these residual IHO1 foci (50%) and the majority of MEI4 foci (63%) co-localized in leptotene *Hormad1*^{−/−} spermatocytes (Fig. 7c–e). Co-localization was similar in a *Spo11*^{−/−} background where both MEI4 and IHO1 foci appeared more stable (Fig. 7f–h).

In yeast two-hybrid assays with known murine DSB-promoting proteins, HORMAD1 interacted only with IHO1 but IHO1 also interacted with REC114, which is a conserved binding partner of MEI4 (Fig. 8a and Supplementary Fig. 7a–d). REC114 is an assumed constituent of DSB-promoting recombinosomes in mammals based on functions of non-mammalian orthologues^{19–22,43}. We also found that IHO1, REC114 and MEI4 self-interacted, which may help in forming cytologically detectable multiprotein assemblies.

The two-hybrid interaction map suggests that REC114 connects MEI4 to IHO1 in DSB-promoting recombinosomes that interact with unsynapsed axis-bound HORMAD1 through HORMAD1–IHO1 linkages. We have thus far been unable to detect soluble complexes of recombinant REC114 and IHO1 in pulldown assays, or soluble complexes of MEI4, REC114 and IHO1 in anti-MEI4 and anti-IHO1 immunoprecipitates of testis extracts, so the putative MEI4-REC114-IHO1 complexes might be transient or their robust formation may require additional insoluble factors in a chromatin context. Therefore, to test whether REC114 is part of MEI4-IHO1-containing complexes *in vivo*, we examined REC114 localization in spermatocytes. An anti-REC114 antibody detected

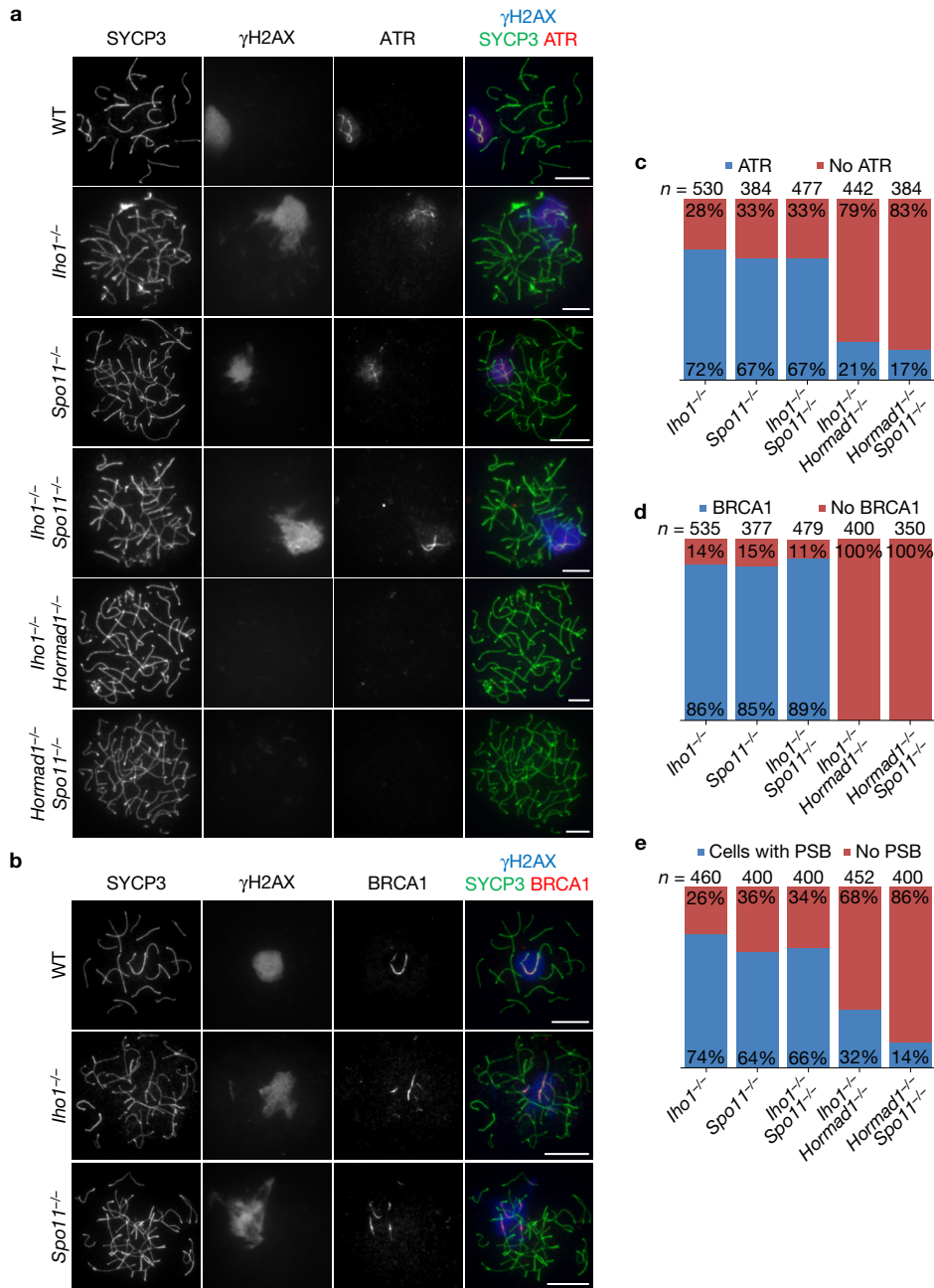


Figure 5 *IHO1* is not required for ATR, BRCA1 or γ H2AX accumulation on unsynapsed chromatin. (a,b) SYCP3, γ H2AX and either ATR (a) or BRCA1 (b) were detected by immunofluorescence on nuclear surface spreads of wild-type (WT) pachytene and mutant zygote-pachytene spermatocytes. Scale bars, 10 μ m. (a) γ H2AX accumulates on sex chromatin in wild type, and on distinct chromatin domains called pseudo-sex bodies in *Iho1*^{-/-}, *Spo11*^{-/-}, and *Iho1*^{-/-}*Spo11*^{-/-}. ATR accumulates both on axes and chromatin loops within these γ H2AX-rich chromatin domains. In contrast, neither γ H2AX nor ATR accumulates in a distinct chromatin domain in the shown *Iho1*^{-/-}*Hormad1*^{-/-} and *Hormad1*^{-/-}*Spo11*^{-/-} spermatocytes. (b) BRCA1 accumulates on axes in pseudo-sex bodies in *Iho1*^{-/-} and *Spo11*^{-/-} spermatocytes. (c–e) Quantification of the fraction of

zygotene-pachytene spermatocytes where ATR (c), or BRCA1 (d) accumulated on unsynapsed chromatin or axis, respectively, or where a pseudo-sex body(ies) (PSB) formed (e). Numbers of counted spermatocytes (*n*) are shown in the combined data sets from two experiments. In *Iho1*^{-/-}, *Spo11*^{-/-} and *Iho1*^{-/-}*Spo11*^{-/-}, ATR-rich chromatin domains (c) and pseudo-sex bodies (e) are frequently observed, and BRCA1 (d) frequently associates with unsynapsed axes in these chromatin domains. In contrast, ATR (c) is absent from chromatin, and pseudo-sex bodies (e) do not form in most *Iho1*^{-/-}*Hormad1*^{-/-} and *Hormad1*^{-/-}*Spo11*^{-/-} spermatocytes. BRCA1 localization to axes (d) was never observed in these two mutants. Primary source data of graphs in c–e are available in Supplementary Table 2.

foci on chromatin in preleptotene; these foci preferentially associated with unsynapsed axes from leptotene onwards and progressively disappeared as chromosomes synapsed and cells proceeded to

pachytene (*n* = 200 cells, Fig. 8b and Supplementary Fig. 7e–g). The majority of REC114 foci co-localized with MEI4 foci in leptotene spermatocytes of both wild-type (62%) and *Hormad1*^{-/-} (53%) mice

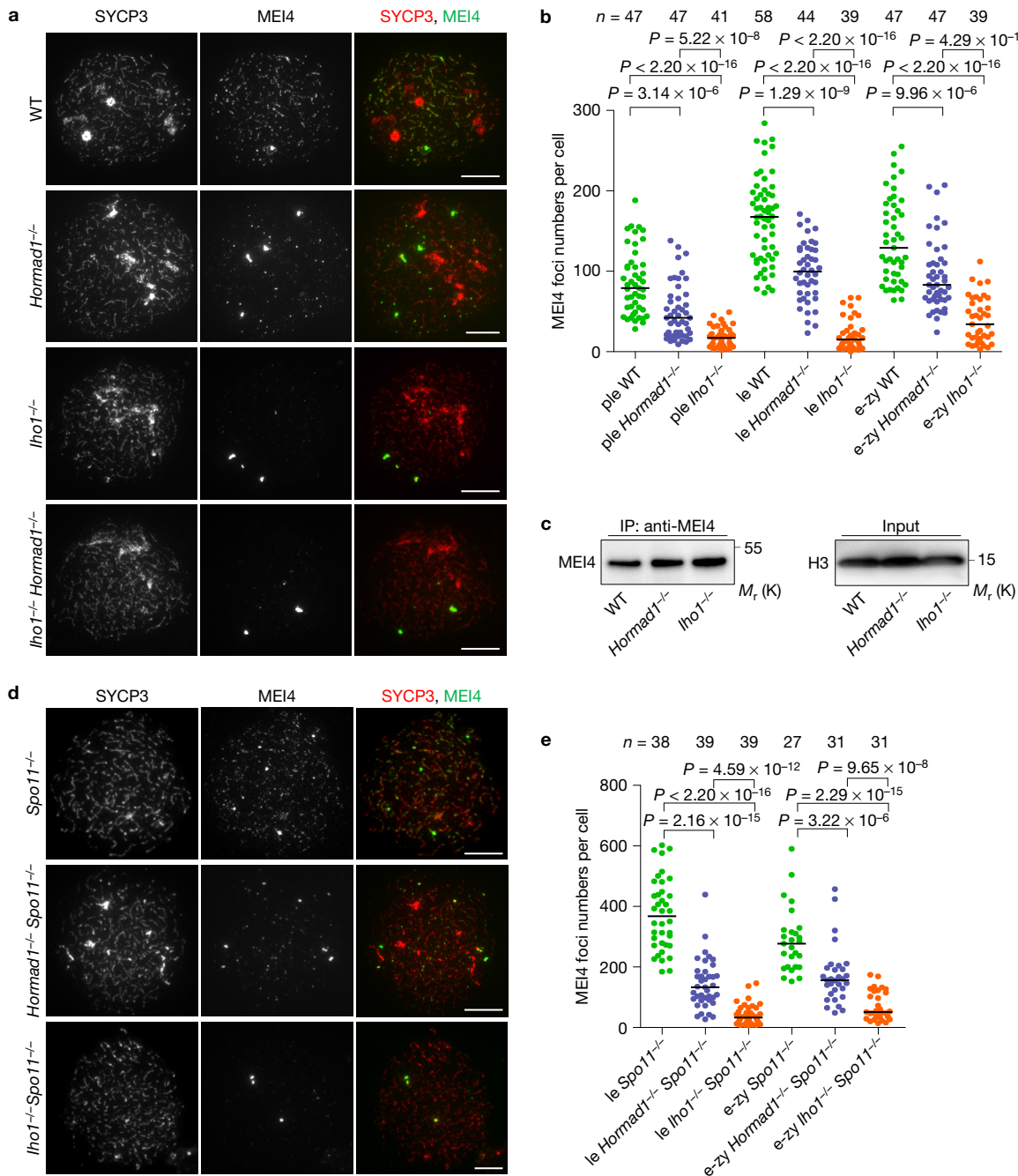


Figure 6 Robust MEI4 focus formation requires IHO1. **(a,d)** MEI4 and SYCP3 were detected in surface spread leptotene spermatocytes of the indicated genotypes. Foci of MEI4 were preferentially detected on the forming axis both in wild type (WT) **(a)** and *Spo11*^{-/-} **(d)**. MEI4 foci were present in lower numbers or were nearly absent in spermatocytes that lacked HORMAD1 or IHO1, respectively, in both *Spo11*^{+/+} **(a)** and *Spo11*^{-/-} **(d)** backgrounds. MEI4 foci were also nearly absent in *Iho1*^{-/-} *Hormad1*^{-/-}, indicating that IHO1 is needed for MEI4 focus formation in *Hormad1*^{-/-}. Scale bars, 10 μ m. **(b,e)** Quantification of MEI4 focus numbers in spermatocytes. Stages: preleptotene (ple), leptotene (le) and early zygote (e-z). Median focus numbers are marked, and n values indicate the number of analysed spermatocytes. Pooled results from three **(b)** or two **(e)** experiments are shown. As MEI4 foci are less robust in *Spo11*^{+/+} than in the *Spo11*^{-/-} background, we detected MEI4 with both guinea pig and rabbit anti-MEI4 antibodies, and counted foci of MEI4 that were detected by both antibodies in the *Spo11*^{+/+} background **(b)**. This strategy increases the chance that the

counted foci represent genuine chromatin-bound MEI4 protein complexes and may explain differences in MEI4 focus counts between the current and previous studies^{16,23} **(e)**. Due to the higher signal-to-noise ratio of MEI4 staining in the *Spo11*^{-/-} background, counts were based only on rabbit anti-MEI4 staining. MEI4 focus numbers were significantly lower in *Hormad1*^{-/-} than in wild type, and were significantly lower in *Iho1*^{-/-} than in wild type or *Hormad1*^{-/-} in both *Spo11*^{+/+} **(b)** and *Spo11*^{-/-} **(e)** backgrounds (Mann–Whitney test). **(c)** MEI4 was immunoprecipitated (IP) from 13 days postpartum mice using anti-MEI4 antibodies crosslinked to magnetic beads. The same antibody was used to detect immunoprecipitated MEI4 by western blot (left image). Detection of histone H3 in the input served as a loading control (right image). MEI4 levels were not lower in *Iho1*^{-/-} (or *Hormad1*^{-/-}) than in wild type. Data represent one out of three experiments. Unprocessed original scans of gels are shown Supplementary Fig. 8. Primary source data of MEI4 focus counts **(b,e)** and MEI4 signal quantification **(c)** are shown in Supplementary Table 2.

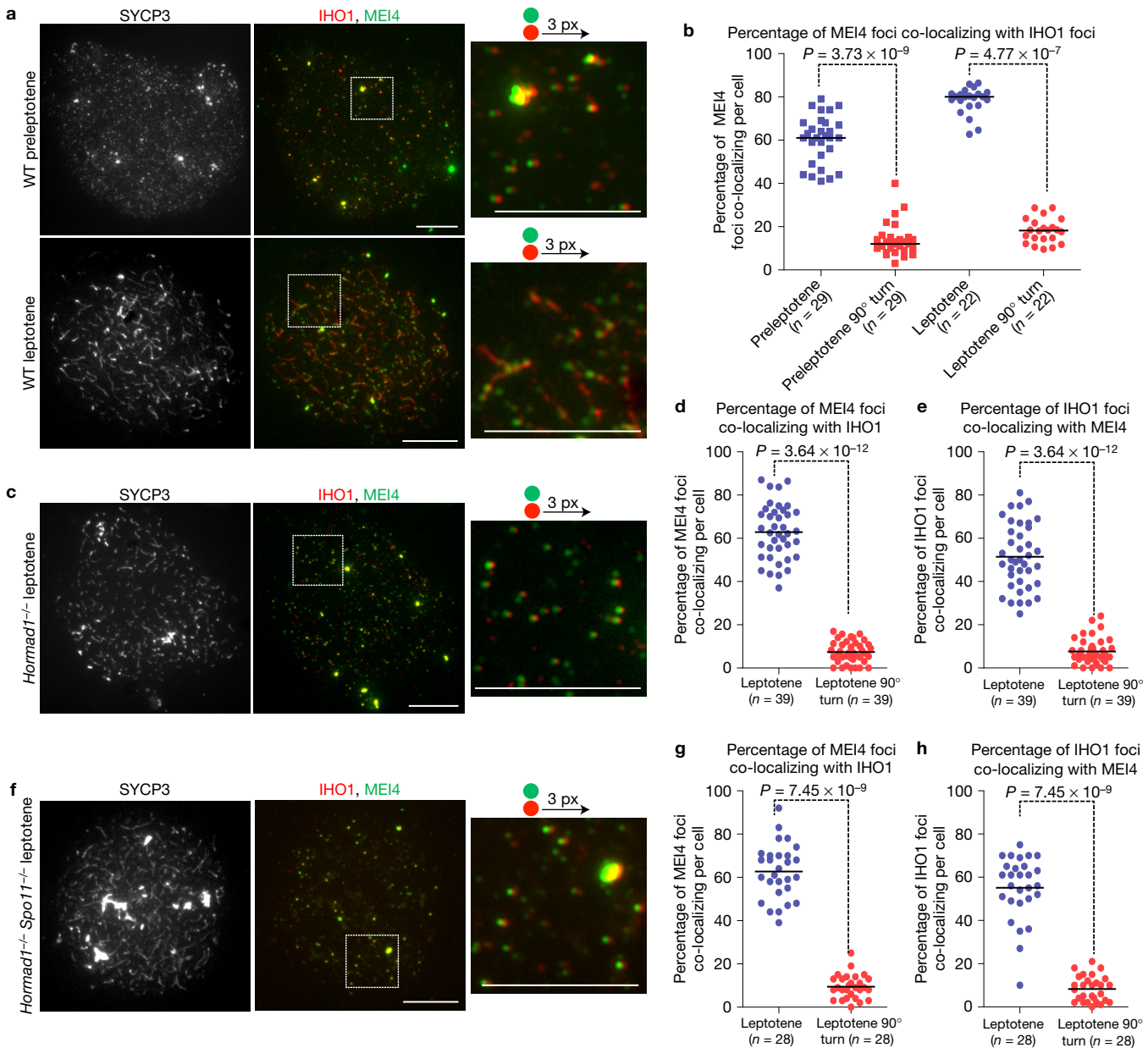


Figure 7 MEI4 and IHO1 co-localize on unsynapsed chromosome axes. **(a,c,f)** MEI4, IHO1 and SYCP3 were detected by immunofluorescence on nuclear surface spreads of wild-type **(a)**, *Hormad1^{-/-}* **(c)** and *Hormad1^{-/-} Spo11^{-/-}* **(f)** spermatocytes. Enlarged insets (right) show co-localization of MEI4 with IHO1 in wild type, *Hormad1^{-/-}* and *Hormad1^{-/-} Spo11^{-/-}*. Note that IHO1 has a ‘spread out’ localization pattern along chromosome axes, whereas MEI4 forms only foci in wild-type leptotene cells. The red channel is shifted to the right by three pixels (px) to allow better visualization of co-localizing green and red signals in the enlarged insets. Scale bars, 10 μm. **(b,d,g)** Quantification of the fractions of MEI4 foci that co-localize with IHO1 foci or stretches (the latter only in wild-type leptotene cells) in wild-type preleptotene and leptotene **(b)**, or *Hormad1^{-/-}* **(d)** and

Hormad1^{-/-} Spo11^{-/-} **(g)** leptotene spermatocytes. **(e,h)** Quantification of the fractions of IHO1 foci that co-localize with MEI4 foci in *Hormad1^{-/-}* **(e)** and *Hormad1^{-/-} Spo11^{-/-}* **(h)** leptotene spermatocytes (same cells were analysed as in **d** and **g**, respectively). To control for random overlap between anti-IHO1 and anti-MEI4 signals, the co-localization frequency was measured with and without rotating the IHO1 image 90° clockwise relative to the MEI4 image. The significantly lower (Mann–Whitney test) co-localization frequency after rotation indicates that MEI4 and IHO1 genuinely co-localize in spermatocytes. Pooled results from two repeats are shown for each experiment, median of co-localization frequency is marked, and *n* indicates the number of analysed nuclei in **b,d,e,g,h**. Primary source data of graphs are shown in Supplementary Table 2.

(Supplementary Fig. 7g–l). Robust anti-REC114 focus formation on chromatin, but not REC114 protein stability, required IHO1 (Fig. 8b–d). Triple immunofluorescence simultaneous staining of MEI4, REC114 and IHO1 displayed extensive co-localization in preleptotene cells (~50% of each protein’s foci; Fig. 8e,f). Co-foci of

MEI4 and REC114 also localized along IHO1-rich unsynapsed axes at later stages (Fig. 8e lower panel). Considering technical limitations in identifying genuine chromatin-associated MEI4 foci, the measured co-localization appears highly significant. The combination of these observations supports the hypothesis that MEI4, REC114 and IHO1

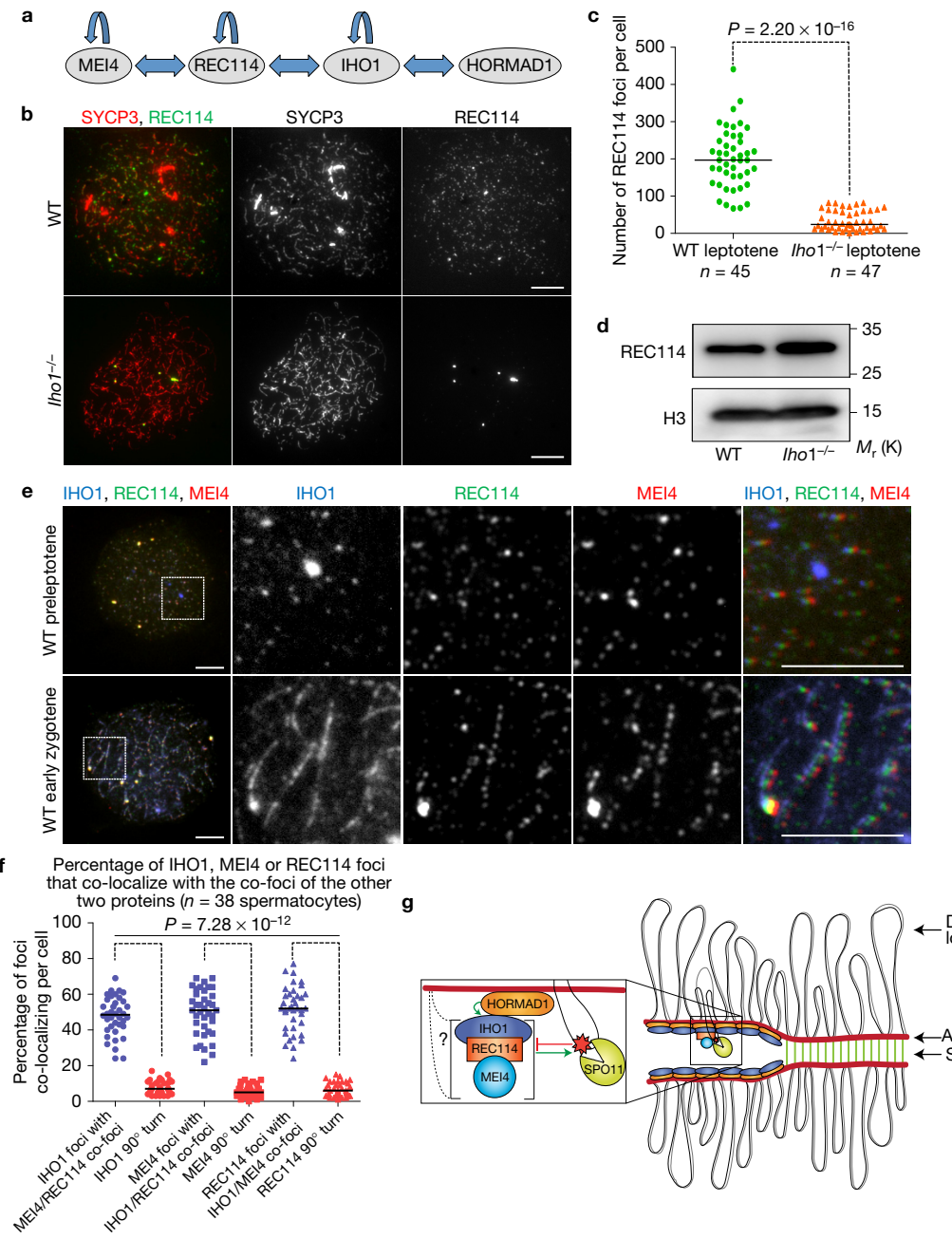


Figure 8 IHO1 is a key component of putative DSB-promoting recombinosomes. **(a)** Schematic depicting yeast two-hybrid interactions between MEI4, REC114, IHO1 and HORMAD1. **(b)** SYCP3 and REC114 were detected in nuclear spreads of wild-type (WT) and *Iho1*^{-/-} leptotene spermatocytes. **(c)** Quantification of REC114 foci showed significantly less REC114 foci in *Iho1*^{-/-} than in wild type (Mann–Whitney test). **(d)** REC114 and histone H3 (loading control) were detected in testis extracts of wild-type and *Iho1*^{-/-} 13 days postpartum mice. REC114 levels were not lower in *Iho1*^{-/-} than in wild type (data represent one out of three experiments, see quantification in Supplementary Table 2). Unprocessed original scans of gels are shown in Supplementary Fig. 8. **(e)** IHO1, REC114 and MEI4 were detected on spreads of wild-type preleptotene or zygotene spermatocytes. Green and red channels are shifted by three and six pixels to the right, respectively, to allow better visualization of co-localizing signals in the enlarged insets. REC114 and MEI4 foci co-localize with IHO1 foci or stretches in preleptotene and zygotene, respectively. Scale bars in **b** and **e**, 10 μm. **(f)** Quantification of co-localization of IHO1, REC114 or MEI4 foci with co-foci of the other two proteins in wild-type preleptotene spermatocytes. Co-localization

was measured with and without rotating IHO1, REC114 or MEI4 images by 90° clockwise to control for random co-localization. Strongly reduced co-localization after rotation (Mann–Whitney test) indicates genuine co-localization of MEI4, REC114 and IHO1. In **c,f**, pools of two repeats are shown, and medians are marked; see Supplementary Table 2 for source data. **(g)** Model for DSB formation in mammalian meiosis. The green arrows and the red blocking arrow indicate promotion and inhibition, respectively. IHO1–REC114 and REC114–MEI4 interactions result in the formation of DSB-promoting recombinosomes that activate SPO11. Signalling from broken DNA ends is thought to prevent repeated DSB formation at nearby sites^{7,49}, possibly by inhibiting or destabilizing DSB-promoting recombinosomes. MEI4–REC114–IHO1 recombinosomes connect to chromosome axes through IHO1–HORMAD1 interaction and as yet unidentified mechanisms (left, question mark). The IHO1–HORMAD1 interaction promotes recruitment of IHO1 and assembly or stabilization of DSB-promoting recombinosomes selectively along unsynapsed axes. This provides one likely, but not exclusive, mechanism for focusing DSB formation on unsynapsed regions, where additional DSBs are needed to promote completion of homologue engagement.

are components of putative DSB-promoting recombinosomes that form on chromatin at the onset of meiosis.

DISCUSSION

Here, we identified the previously uncharacterized IHO1 as a HORMAD1-interacting protein that is essential for DSB formation but not for HORMAD1 functions in pairing-independent SC formation, ATR recruitment to unsynapsed axes, MSUC, or meiotic surveillance. MEI4, REC114 and IHO1 form chromatin-bound complexes that appear crucial for DSB formation. These results are consistent with functions of the presumed Spo11-activating complex in yeast containing Mei4 and Rec114 plus a coiled-coil protein that lacks primary sequence conservation between fission (Rec15) and budding (Mer2) yeasts^{9,19–22}. This complex (hereafter the MCD recombinosome: MEI4-containing DSB-promoting) interacts with Spo11 through intermediary proteins^{9,20–22}. MCD recombinosomes may link Spo11 activity to the chromosome axis because chromatin immunoprecipitates of yeast MCD recombinosome components are enriched in DNA sequences that also associate with axis components^{18,21}. Curiously, although there are no clear IHO1 orthologues beyond vertebrates, IHO1 is also a coiled-coil protein. Thus, we hypothesize that IHO1 is a functional equivalent of Mer2/Rec15 and that SPO11 activity depends on a conserved MCD recombinosome in mice as in yeasts.

There is functional interplay between the axis and MCD recombinosomes for which HORMA-domain proteins are important, particularly in budding yeast¹⁸ and mice¹⁶, but to a lesser extent in fission yeast^{44,45}. HORMA-domain proteins are needed for robust accumulation of MCD recombinosome components on chromatin and axes in mice (ref. 16 and this study), and on axis-binding DNA regions in budding yeast¹⁸. MCD recombinosome components are essential for DSB formation, whereas meiotic HORMA-domain proteins are only partially necessary⁹. Correspondingly, MCD recombinosomes were still observed in *Hormad1*^{−/−} spermatocytes in mice, albeit at reduced numbers (ref. 16 and this study). HORMA-domain proteins may thus act by enhancing the essential function of MCD recombinosomes. Our epistasis experiments between *Hormad1* and *Iho1* tested this hypothesis, revealing that both DSB formation and residual MEI4 focus formation in *Hormad1*^{−/−} spermatocytes depend on IHO1. Thus, IHO1 can promote DSB formation independently of HORMAD1, probably as part of the MCD recombinosome. Conversely, our observations support the idea that HORMAD1 promotes DSB formation by fostering assembly or stabilization of MCD recombinosomes. We hypothesize that HORMAD1 performs its DSB-promoting function through its interaction with IHO1, revealed by yeast two-hybrid, co-immunoprecipitation, and co-localization. HORMAD1 may induce conformational changes in IHO1 via direct binding, or HORMAD1-mediated recruitment of unidentified enzymatic activities may lead to activating modifications of MCD recombinosome components. HORMAD1 is required for ‘spread out’ IHO1 localization along unsynapsed axes, but MEI4, REC114 and IHO1 form foci along unsynapsed axes even in the absence of HORMAD1, so IHO1–HORMAD1 interaction is not the sole link between MCD recombinosomes and axes (Fig. 8g). The nature of this HORMAD1-independent recruitment is unclear, but it may involve another known DSB-promoting protein, MEI1 (ref. 46),

because MEI4 foci do not associate robustly with axes in the absence of MEI1 even in a HORMAD1-proficient background¹⁶. This suggests that the primary function of IHO1–HORMAD1 interaction is not MCD-recombinosome recruitment to axes, but may instead be to support assembly or stabilization of MCD recombinosomes.

A model for the linkage of DSB formation to unsynapsed chromosome axes in mammals is presented in Fig. 8g. Pairwise interactions between IHO1–REC114 and REC114–MEI4 assemble chromatin-bound recombinosomes that promote DSB formation by activating SPO11 through an as yet unidentified mechanism. Robust assembly and/or stabilization of MCD recombinosomes require HORMAD1 starting from preleptotene, before distinguishable axis structures have formed. Parallel to DSB formation—presumably reliant on this initial set of MCD recombinosomes—axes form and HORMAD1 recruits IHO1 to elongating unsynapsed axes. This probably provides a platform for selective assembly and stabilization of additional MCD recombinosomes specifically along unsynapsed axes, where further DSB formation is desirable for successful homologue alignment. Following SC formation, however, HORMAD1 becomes depleted from axes. HORMAD1 depletion is a likely, but not sole, mechanism to protect against excessive DSB formation by destabilizing MCD recombinosomes in regions where DSBs are no longer needed for homology search. IHO1 is removed more efficiently than HORMAD1 from synapsed axes, indicating that HORMAD1 displacement is not the only means by which SC formation displaces IHO1 and MCD recombinosomes. Additional mechanisms may include disruption of the IHO1–HORMAD1 interaction, localized degradation, and/or inactivating post-translational modifications of MCD recombinosome components.

DSB formation is no longer needed in pachytene, and IHO1 disappears even from unsynapsed axes in spermatocytes through an unknown mechanism. IHO1 disappearance may also bring DSB formation to a halt on unsynapsed sex chromosome axes in pachytene. Curiously, IHO1 reappears in spermatocytes both on unsynapsed sex chromosomes and on desynapsing autosomes in late pachytene and diplotene, respectively. Apoptosis of *Iho1*^{−/−} spermatocytes at a mid-pachytene-equivalent stage precluded examining IHO1 functions at these late stages, where DSBs no longer form. Selective depletion after IHO1 performed its essential functions in DSB formation will be necessary to address possible late functions in spermatocytes. □

METHODS

Methods, including statements of data availability and any associated accession codes and references, are available in the online version of this paper.

Note: Supplementary Information is available in the online version of the paper

ACKNOWLEDGEMENTS

We thank R. Jessberger (Institute of Physiological Chemistry, Faculty of Medicine at the TU Dresden, Germany) for sharing ideas, antibodies (anti-SYCP3 and anti-STAG3) and departmental support; M. Stevenson for discussion, and revising and proofreading the manuscript; G. Vader (Department of Mechanistic Cell Biology, Max Planck Institute of Molecular Physiology, Dortmund, Germany) for sharing budding yeast protocols; E. Marcon (Donnelly Centre, University of Toronto, Canada) for the anti-RPA antibody; F. Schwarz (Genomics and Proteomics Core Facilities, German Cancer Research Center–DKFZ, Germany) and the protein interaction unit of Genomics and Proteomics Core Facility at the German Cancer Research Center–DKFZ for yeast two-hybrid vectors and for performing yeast

two-hybrid screens; M. P. Thelen (Physical and Life Sciences Directorate, Lawrence Livermore National Laboratory, USA) for the anti-SPO11 antibody; M. A. Handel (The Jackson Laboratory, USA) for histone H1T antibody; D. Drechsel (Max Planck Institute of Molecular Cell Biology and Genetics, Germany) and the EMBL protein expression and purification facility for protein expression vectors; K. Daniel (Biotechnology Center TU Dresden-BIOTEC, Germany) for testis and somatic tissue cDNAs. We thank the DIGS-BB programme for supporting M.S. The Deutsche Forschungsgemeinschaft (DFG; grants: TO421/3-2, SPP1384:TO421/4-2, TO421/5-1, TO421/6-1, TO421/8-1 and 8-2) supported M.S., M.B., F.P., I.D., A.R., D.T. and A.T.; The JSPS Research Fellowship supported H.S., Y.W.; B.d.M. was funded by grants from the Centre National pour la Recherche Scientifique (CNRS) and the European Research Council Executive Agency under the European Community's Seventh Framework Programme (FP7/2007–2013 Grant Agreement no. [322788]); the NIH (R01 GM105421) supported J.L., M.J. and S.K.; J.L. was supported in part by American Cancer Society fellowship PF-12-157-01-DMC. S.K. is an Investigator of the Howard Hughes Medical Institute.

AUTHOR CONTRIBUTIONS

Most experiments were carried out by M.S. (Figs 1a–c, 4 and 6–8a,d,g and Supplementary Figs 1b,c, 2b,d, 3, 5b–e, 6 and 7a–d) and M.B. (Figs 1e and 3a–f and Supplementary Figs 1a,d,e, 2a,c and 5a,f,h). Further experiments were performed by F.P. (Figs 2 and 5 and Supplementary Figs 4 and 5f,g), I.D. (Figs 1d and 8b,c,e,f and Supplementary Fig. 7e–l) and J.L. (Fig. 3g,h). Knockout embryonic stem cells were generated by D.T. with the supervision of A.R.; M.J. and S.K. contributed to SPO11-oligonucleotide measurements and S.K. supplied REC114 antibodies; B.d.M. supplied MEI4 antibodies, experimental material and critical unpublished information, H.S. and Y.W. contributed with critical supporting IHO1 localization data. A.T. and M.S. wrote the manuscript. All authors were involved in discussions and commented on the manuscript.

COMPETING FINANCIAL INTERESTS

The authors declare no competing financial interests.

Published online at <http://dx.doi.org/10.1038/ncb3417>

Reprints and permissions information is available online at www.nature.com/reprints

- Baudat, F. & de Massy, B. Regulating double-stranded DNA break repair towards crossover or non-crossover during mammalian meiosis. *Chromosome Res.* **15**, 565–577 (2007).
- Hunter, N. *Meiotic Recombination in Molecular Genetics of Recombination* (Springer, 2007).
- Bergerat, A. *et al.* An atypical topoisomerase II from Archaea with implications for meiotic recombination. *Nature* **386**, 414–417 (1997).
- Keeney, S., Giroux, C. N. & Kleckner, N. Meiosis-specific DNA double-strand breaks are catalyzed by Spo11, a member of a widely conserved protein family. *Cell* **88**, 375–384 (1997).
- Wojtasz, L. *et al.* Mouse HORMAD1 and HORMAD2, two conserved meiotic chromosomal proteins, are depleted from synapsed chromosome axes with the help of TRIP13 AAA-ATPase. *PLoS Genet.* **5**, e1000702 (2009).
- Thacker, D., Mohibullah, N., Zhu, X. & Keeney, S. Homologue engagement controls meiotic DNA break number and distribution. *Nature* **510**, 241–246 (2014).
- Keeney, S., Lange, J. & Mohibullah, N. Self-organization of meiotic recombination initiation: general principles and molecular pathways. *Annu. Rev. Genet.* **48**, 187–214 (2014).
- Kauppi, L. *et al.* Numerical constraints and feedback control of double-strand breaks in mouse meiosis. *Genes Dev.* **27**, 873–886 (2013).
- Lam, I. & Keeney, S. Mechanism and regulation of meiotic recombination initiation. *Cold Spring Harb. Perspect. Biol.* **7**, a016634 (2015).
- Rosenberg, S. C. & Corbett, K. D. The multifaceted roles of the HORMA domain in cellular signaling. *J. Cell Biol.* **211**, 745–755 (2015).
- Fukuda, T., Daniel, K., Wojtasz, L., Toth, A. & Hoog, C. A novel mammalian HORMA domain-containing protein, HORMAD1, preferentially associates with unsynapsed meiotic chromosomes. *Exp. Cell Res.* **316**, 158–171 (2010).
- Daniel, K. *et al.* Meiotic homologue alignment and its quality surveillance are controlled by mouse HORMAD1. *Nat. Cell Biol.* **13**, 599–U232 (2011).
- Kogo, H. *et al.* HORMAD1-dependent checkpoint/surveillance mechanism eliminates asynchronous oocytes. *Genes Cells* **17**, 439–454 (2012).
- Shin, Y. H. *et al.* Hormad1 mutation disrupts synaptonemal complex formation, recombination, and chromosome segregation in mammalian meiosis. *PLoS Genet.* **6**, e1001190 (2010).
- Shin, Y. H., McGuire, M. M. & Rajkovic, A. Mouse HORMAD1 is a meiosis I checkpoint protein that modulates DNA double-strand break repair during female meiosis. *Biol. Reprod.* **89**, 29 (2013).
- Kumar, R. *et al.* MEI4: a central player in the regulation of meiotic DNA double strand break formation in the mouse. *J. Cell Sci.* **128**, 1800–1811 (2015).
- Blat, Y., Protacio, R. U., Hunter, N. & Kleckner, N. Physical and functional interactions among basic chromosome organizational features govern early steps of meiotic chiasma formation. *Cell* **111**, 791–802 (2002).
- Panizza, S. *et al.* Spo11-accessory proteins link double-strand break sites to the chromosome axis in early meiotic recombination. *Cell* **146**, 372–383 (2011).
- Li, J., Hooker, G. W. & Roeder, G. S. *Saccharomyces cerevisiae* Mer2, Mei4 and Rec114 form a complex required for meiotic double-strand break formation. *Genetics* **173**, 1969–1981 (2006).
- Maleki, S., Neale, M. J., Arora, C., Henderson, K. A. & Keeney, S. Interactions between Mei4, Rec114, and other proteins required for meiotic DNA double-strand break formation in *Saccharomyces cerevisiae*. *Chromosoma* **116**, 471–486 (2007).
- Miyoshi, T. *et al.* A central coupler for recombination initiation linking chromosome architecture to S phase checkpoint. *Mol. Cell* **47**, 722–733 (2012).
- Arora, C., Kee, K., Maleki, S. & Keeney, S. Antiviral protein Ski8 is a direct partner of Spo11 in meiotic DNA break formation, independent of its cytoplasmic role in RNA metabolism. *Mol. Cell* **13**, 549–559 (2004).
- Kumar, R., Bourbon, H. M. & de Massy, B. Functional conservation of Mei4 for meiotic DNA double-strand break formation from yeasts to mice. *Genes Dev.* **24**, 1266–1280 (2010).
- Lin, S. *et al.* Comparison of the transcriptional landscapes between human and mouse tissues. *Proc. Natl. Acad. Sci. USA* **111**, 17224–17229 (2014).
- Yue, F. *et al.* A comparative encyclopedia of DNA elements in the mouse genome. *Nature* **515**, 355–364 (2014).
- Burgoyne, P. S., Mahadevaiah, S. K. & Turner, J. M. The consequences of asynapsis for mammalian meiosis. *Nat. Rev. Genet.* **10**, 207–216 (2009).
- Barchi, M. *et al.* Surveillance of different recombination defects in mouse spermatocytes yields distinct responses despite elimination at an identical developmental stage. *Mol. Cell. Biol.* **25**, 7203–7215 (2005).
- Pacheco, S. *et al.* The ATM signaling cascade promotes recombination-dependent pachytene arrest in mouse spermatocytes. *PLoS Genet.* **11**, e1005017 (2015).
- Mahadevaiah, S. K. *et al.* Extensive meiotic asynapsis in mice antagonizes meiotic silencing of unsynapsed chromatin and consequently disrupts meiotic sex chromosome inactivation. *J. Cell Biol.* **182**, 263–276 (2008).
- Neale, M. J., Pan, J. & Keeney, S. Endonucleolytic processing of covalent protein-linked DNA double-strand breaks. *Nature* **436**, 1053–1057 (2005).
- Pittman, D. L. *et al.* Meiotic prophase arrest with failure of chromosome synapsis in mice deficient for *Dmc1*, a germline-specific *RecA* homolog. *Mol. Cell* **1**, 697–705 (1998).
- Yoshida, K. *et al.* The mouse *RecA*-like gene *Dmc1* is required for homologous chromosome synapsis during meiosis. *Mol. Cell* **1**, 707–718 (1998).
- Kogo, H. *et al.* HORMAD2 is essential for synapsis surveillance during meiotic prophase via the recruitment of ATR activity. *Genes Cells* **17**, 897–912 (2012).
- Wojtasz, L. *et al.* Meiotic DNA double-strand breaks and chromosome asynapsis in mice are monitored by distinct HORMAD2-independent and -dependent mechanisms. *Genes Dev.* **26**, 958–973 (2012).
- Turner, J. M. *et al.* BRCA1, histone H2AX phosphorylation, and male meiotic sex chromosome inactivation. *Curr. Biol.* **14**, 2135–2142 (2004).
- Royo, H. *et al.* ATR acts stage specifically to regulate multiple aspects of mammalian meiotic silencing. *Genes Dev.* **27**, 1484–1494 (2013).
- Turner, J. M., Mahadevaiah, S. K., Ellis, P. J., Mitchell, M. J. & Burgoyne, P. S. Pachytene asynapsis drives meiotic sex chromosome inactivation and leads to substantial postmeiotic repression in spermatids. *Dev. Cell* **10**, 521–529 (2006).
- Turner, J. M. *et al.* Silencing of unsynapsed meiotic chromosomes in the mouse. *Nat. Genet.* **37**, 41–47 (2005).
- Royo, H. *et al.* Evidence that meiotic sex chromosome inactivation is essential for male fertility. *Curr. Biol.* **20**, 2117–2123 (2010).
- Bellani, M. A., Romanienko, P. J., Cairatti, D. A. & Camerini-Otero, R. D. SPO11 is required for sex-body formation, and *Spo11* heterozygosity rescues the prophase arrest of *Atm*^{−/−} spermatocytes. *J. Cell Sci.* **118**, 3233–3245 (2005).
- Cloutier, J. M. *et al.* Histone H2AFX links meiotic chromosome asynapsis to prophase I oocyte loss in mammals. *PLoS Genet.* **11**, e1005462 (2015).
- Carballo, J. A., Johnson, A. L., Sedgwick, S. G. & Cha, R. S. Phosphorylation of the axial element protein Hop1 by Mec1/Tel1 ensures meiotic interhomolog recombination. *Cell* **132**, 758–770 (2008).
- Sasanuma, H. *et al.* Meiotic association between Spo11 regulated by Rec102, Rec104 and Rec114. *Nucleic Acids Res.* **35**, 1119–1133 (2007).
- Latypov, V. *et al.* Roles of Hop1 and Mek1 in meiotic chromosome pairing and recombination partner choice in *Schizosaccharomyces pombe*. *Mol. Cell. Biol.* **30**, 1570–1581 (2010).
- Lorenz, A., Estreicher, A., Kohli, J. & Loidl, J. Meiotic recombination proteins localize to linear elements in *Schizosaccharomyces pombe*. *Chromosoma* **115**, 330–340 (2006).
- Libby, B. J., Reinholdt, L. G. & Schimenti, J. C. Positional cloning and characterization of *Mei1*, a vertebrate-specific gene required for normal meiotic chromosome synapsis in mice. *Proc. Natl. Acad. Sci. USA* **100**, 15706–15711 (2003).
- Bellani, M. A., Boateng, K. A., McLeod, D. & Camerini-Otero, R. D. The expression profile of the major mouse SPO11 isoforms indicates that SPO11β introduces double strand breaks and suggests that SPO11α has an additional role in prophase in both spermatocytes and oocytes. *Mol. Cell. Biol.* **30**, 4391–4403 (2010).
- Romanienko, P. J. & Camerini-Otero, R. D. Cloning, characterization, and localization of mouse and human SPO11. *Genomics* **61**, 156–169 (1999).
- Lange, J. *et al.* ATM controls meiotic double-strand-break formation. *Nature* **479**, 237–240 (2011).

METHODS

Yeast two-hybrid, RNA isolation and RT-PCR. To perform yeast two-hybrid screen, human *Hormad1* full-length gene (Source Bioscience, IMAGE ID: 5298160) was sub-cloned into a *Saccharomyces cerevisiae* yeast two-hybrid bait vector (pNGB, sequence available on request). Full-length HORMAD1 in fusion with C-terminal Gal4-DNA binding domain was used as a bait in combination with two prey libraries: a human testis cDNA library (Mate & Plate Library—Human, 630470, Clontech) and a human full-length open reading frame (ORF) cDNA library (unpublished, DKFZ). The prey libraries were supplied and the screens were performed by the Genome and Proteome Core Facility at the German Cancer Research Center (DKFZ) as described previously⁵⁰. To test pairwise interactions between candidates by yeast two-hybrid (Supplementary Fig. 7a–d) we used published methods with minor modifications⁵¹. Interactions were tested in the Y2HGold Yeast strain (Cat. no. 630498, Clontech). To transform Y2HGold with bait and prey vectors, yeasts were grown in 2xYPDA medium⁵¹ overnight at 30 °C, 200 r.p.m. shaking. Afterwards, yeast cells were diluted to 0.4 optical density (measured at 600 nm) and incubated in 2xYPDA for 5 h at 30 °C, 200 r.p.m. shaking. Cells were harvested, washed with water and resuspended in 2 ml of 100 mM lithium acetate (LiAc). Fifty microlitres of this cell suspension was used for each transformation. Transformation mix included 1 µg of each vector (bait and prey), 60 µl of polyethylene glycol 50% (w/v in water), 9 µl of 1.0 M LiAc, 12.5 µl of boiled single-strand DNA from salmon sperm (AM9680, Ambion), and water up to 90 µl in total. The transformation mix was incubated at 30 °C for 30 min, and then at 42 °C for 30 min for the heat shock. The transformation mix was removed following centrifugation at 1,000g for 10 min, and then cells were resuspended in water, and plated first on -Leu -Trp plates to allow selective growth of transformants. After 2 days of growth transformants were plated both on -Leu -Trp and -Leu -Trp -Ade -His plates for 3–7 days to test for interactions. For media and plate preparation we followed the manufacturer's instructions⁵² (see more at: <http://www.sigmaldrich.com/technical-documents/articles/biology/yeast-drop-out.html#sthash.zJzt2dEy.dpuf>). To test *Iho1* expression in testis and ovaries, RNA was isolated and RT-PCR was performed as described earlier⁵³. The RNA of the somatic tissue mix in Supplementary Fig. 1a originated from 17 distinct tissues: liver, brain, thymus, heart, lung, spleen, kidney, mammary gland, pancreas, placenta, salivary gland, skeletal muscle, skin, small intestine, spinal cord, tongue and uterus.

Generation of knockouts and genotyping. The *Ccdc36*-targeting construct (clone HTGRS6006_A_G10, BACPAC Resources Center, Knockout Mouse Project KOMP repository) was based on a so-called 'knockout first' multipurpose allele strategy⁵⁴ (Supplementary Fig. 3). Targeting of R1 (agouti) embryonic stem cell was carried out as before¹² and chimaeras were generated by laser-assisted C57BL/6 morula injections with embryonic stem cell clones heterozygote for the *Iho1*^{insertion} allele (Supplementary Fig. 3). Progeny of the chimeric animals were crossed to the outbred wild-type CD-1 mouse line, and to pCAGGs-FLPo⁵⁵ and PGK-Cre⁵⁶ transgenic mice to generate first *Iho1*^{restored}, and then *Iho1*^{deletion} alleles from *Iho1*^{insertion} allele (Supplementary Fig. 3). Mice were maintained on the outbred ICR (CD-1) background. Mice were initially genotyped by Southern blotting (Supplementary Fig. 3), and by PCR in subsequent crosses using tail-tip genomic DNAs. Genotyping primers:

LacZfor 5'-CCCGTCGTTTACAACGTC-3'
 LacZrev 5'-CATACCACCAACGCTCATC-3'
*Ccdc36*RestFw 5'-CCAACAATACTCATTACCCC-3'
*Ccdc36*RestRv 5'-ACTATTTACTCTGCCTCTGAGC-3'
*Ccdc36*LoxPRv1 5'-AACTTCAAAACACCTCGCC-3'
 5*Ccdc36*seq2 5'-TCTTCCTTGCCAGTTGGAAATC-3'
*Cre*Fw 5'-GCCTGCATTACCGTCGATGCAACGA-3'
*Cre*Rv 5'-GTGGCAGATGGCGCGAACACCAT-3'
FlpOFw 5'-GCTATCGAATTCCACCATGGCTCTAAAGAA-3'
FlpORv 5'-CAATCGCGATGAATTCTCAGATCCGCCGTTGATGTA-3'

PCR product sizes: with LacZfor/LacZrev primers, *Iho1*^{insertion} template—208 bp, other alleles—no specific product; with *Ccdc36*RestFw/*Ccdc36*RestRv primers, wild-type allele template—357 bp, *Iho1*^{insertion} template—7,423 bp, *Iho1*^{restored} template—500 bp; with 5*Ccdc36*seq2/*Ccdc36*LoxPRv1 primers, wild-type allele template—404 bp, *Iho1*^{insertion} and *Iho1*^{restored} templates—366 bp, *Iho1*^{deletion} template—no specific product; with *Ccdc36*RestFw/*Ccdc36*LoxPRv1 primers: wild-type allele—1,096 bp, *Iho1*^{insertion} template—no specific product, *Iho1*^{restored} template—1,201 bp, *Iho1*^{deletion} template—373 bp. *FlpOFw*/*FlpORv* were used to detect *FlpO* recombinase (1,500 bp); *Cre*Fw/*Cre*Rv were used to detect *Cre* recombinase (750 bp).

Animal experiments. Mice carrying *Hormad1*-, *Spo11*-, *Dmc1*- or *Mei4*-null alleles were described earlier^{12,23,31,57}. Western blotting reconfirmed the absence of full-length IHO1 protein from testis extracts of both *Iho1*^{insertion/insertion} and *Iho1*^{deletion/deletion} mice (Supplementary Fig. 3c). Histology in testis, analysis of the synaptonemal complex and the axis, and focus counts of RAD51, DMC1 and RPA were carried out in both *Iho1*^{insertion} and *Iho1*^{deletion} strains. The rest of the experiments were carried out

in the *Iho1*^{deletion} lineage. As no obvious differences were detected between the strains we refer to both of their genotypes as *Iho1*^{−/−}. *Iho1*^{restored/restored} mice were fertile and their spermatocytes were indistinguishable from wild-type spermatocytes. This supported the specificity of the observed phenotypes in the *Iho1*^{insertion} and *Iho1*^{deletion} strains. Whenever possible, experimental animals were compared with littermate controls or with age-matched non-littermate controls from the same colony. Adult mice between age 70–120 days were used for experiments unless indicated otherwise. No statistical method was used to predetermine sample size. The experiments were not randomized. The investigators were not blinded to allocation during experiments and outcome assessment. All animals were used and maintained in accordance with the German Animal Welfare legislation ('Tierschutzgesetz'). All procedures pertaining to animal experiments were approved by the Governmental IACUC ('Landesdirektion Sachsen') and overseen by the animal ethics committee of the Technische Universität Dresden. The licence numbers concerned with the present experiments with mice are DD24-5131/287/1 and 24-9168.24-1/2006-13 (tissue collection without prior *in vivo* experimentation).

Cell lines. Only the R1 embryonic stem cell line was used in this study. This cell line was not found in the database of commonly misidentified cell lines that is maintained by ICLAC and NCBI Biosample. The cell line was not authenticated. The cell line was not tested for mycoplasma contamination.

Antibody generation. To produce anti-IHO1 antibody, full-length mouse *Ccdc36* (*Iho1*) open reading frame and four non-overlapping fragments that together covered the full-length *Ccdc36* open reading frame were sub-cloned from plasmid DNA (Source Bioscience, IMAGE ID: 5716219) into *Escherichia coli* expression vectors pDEST17 (Cat. no. 11803-012, Invitrogen) and petMM30 (gift from D. Drechsel, sequence available on request), respectively. These expression vectors were used to produce N-terminal 6xHis-tagged full-length IHO1, and 6xHis-1xGST-tagged IHO1 fragments in bacteria. All recombinant proteins were purified on Ni-Sepharose beads (Cat. no. 17-5318-01, Amersham, GE Healthcare), and the tagged full-length IHO1 preparations were used for immunization of rabbits, guinea pigs and chickens. Polyclonal anti-IHO1 antibodies were affinity purified on antigen-coupled NHS-Activated Sepharose 4 Fast Flow beads (Cat. no. 17-0906-01, Amersham, GE Healthcare) according to standard methods⁵⁸. Guinea pig and chicken anti-IHO1 serum was purified using IHO1 full-length recombinant protein; rabbit anti-IHO1 serum was purified first using IHO1 full-length and subsequently using recombinant IHO1-fragment peptides. Antibodies specific to IHO1 fragment-1 (144 amino acids from Met1 to Val144) produced the best signal-to-noise ratio in immunofluorescence; hence, we used this antibody in most IHO1 localization experiments where rabbit anti-IHO1 antibody was used. All antibodies were tested by immunofluorescence staining of spermatocyte nuclear spreads. Antibodies from all three species showed a similar staining pattern. The localization pattern of IHO1 was also reconfirmed by overexpression of a GFP-tagged version of IHO1 following *in vivo* electroporation of testes^{59,60}. In addition, all antibodies were tested by immunoblot analysis of testis extracts. Although all of the antibodies recognized several proteins of different molecular weights, only a protein with a relative molecular mass of approximately 65,000 (M_r ~65k) based on its electrophoretic mobility was absent from *Iho1*^{−/−} testis extracts (Supplementary Fig. 3c), and was detected by all the different antibodies in wild-type testis extracts. The size of this protein corresponds well to the predicted molecular mass of IHO1 (M_r 63.4 kDa).

To produce anti-MEI4 antibody, mouse full-length *Mei4* open reading frame and two non-overlapping fragments corresponding to the N-terminal (130 amino acids: Met1 to Leu130) and C-terminal (129 amino acids: Arg261 to Pro389) parts of MEI4 were sub-cloned from plasmid DNA²³ into *Escherichia coli* expression vectors pDEST17, for full-length *Mei4*, or pETG41A (EMBL protein expression and purification facility), for both fragments. These expression vectors were used to produce N-terminal 6xHis-tagged full-length MEI4 and 6xHis-1xMBP-tagged MEI4 fragments in bacteria. The recombinant full-length MEI4 protein and MEI4 fragments were purified on Ni-Sepharose beads (Cat. no. 17-5318-01, Amersham, GE Healthcare) and 6xHis-tagged full-length MEI4 protein was used for immunization of guinea pigs. Polyclonal anti-MEI4 antibodies were affinity purified on antigen-coupled NHS-activated Sepharose 4 fast flow beads (Cat. no. 17-0906-01, Amersham, GE Healthcare). Guinea pig anti-MEI4 serum was purified first using MEI4 full-length, and subsequently using recombinant MEI4-fragment peptides. Antibodies specific to MEI4 fragment-1 (130 amino acids from Met1 to Leu130) produced the best signal-to-noise ratio in immunofluorescence; hence, we used this antibody in most MEI4 localization experiments. The specificity of the MEI4 fragment-1 antibody was tested by co-immunostaining wild-type and *Mei4*^{−/−} spermatocyte nuclear spreads with the anti-MEI4 fragment-1 antibody and a published rabbit anti-MEI4 antibody²³. The two antibodies showed similar staining patterns, and numbers of foci detected by both antibodies were dramatically reduced in *Mei4*^{−/−} as compared with wild-type spermatocytes. Medians of focus numbers detected by the new guinea pig and the published²³ rabbit antibodies

were 5 and 47, respectively, and the median of co-focus numbers was 1 in *Mei4^{-/-}* spermatocytes ($n=36$ leptotene spermatocytes; Supplementary Table 2, 'gp&rb MEI4 WTvsMEI4ko'). Medians of focus numbers detected by the new guinea pig and the published rabbit antibodies were 304 and 361, respectively, and the median of co-focus numbers was 220 in wild-type spermatocytes ($n=29$ spermatocytes; Supplementary Table 2, 'gp&rb MEI4 WTvsMEI4ko'). In addition, the guinea pig anti-MEI4 fragment-1 antibody was tested in immunoprecipitation and immunoblot analysis of testis extracts. This antibody recognizes a protein of approximately M_r 50K based on its electrophoretic mobility (Fig. 6c), which corresponds well to the predicted molecular mass of MEI4 (M_r , 44.5K).

Other antibodies. In addition to antibodies that were previously described^{5,12}, we used: rabbit anti-MEI4 (ref. 23) (immunofluorescence (IF) 1:50), guinea pig anti-MEI4 (IF 1:500, western blotting (WB) 1:2,000), rabbit anti-REC114 (IF 1:500, WB 1:2,000, unpublished antibody of S.K. and M. van Overbeek (Molecular Biology Program, Memorial Sloan Kettering Cancer Center, USA; current affiliation: Caribou Biosciences, USA)), guinea pig anti-IHO1 (IF 1:2,000), rabbit anti-IHO1 fragment-1 (IF 1:2,000, WB 1:3,000), chicken anti-IHO1 (IF 1:3,000), goat anti-Beta actin (WB 1:1,000, ab8229 from Abcam), rabbit anti-SYCP3 (WB 1:6,000, ab15093 from Abcam).

Immunofluorescence microscopy. Preparation and immunostaining of testis–ovary cryosections and nuclear surface spreads of meiocytes were adapted from methods described previously with minor modifications⁶¹. Briefly, testis cell suspensions were prepared in PBS pH 7.4, then mixed with hypotonic extraction buffer in 1:1 ratio and incubated for 8 min at room temperature. After diluting the cell suspension five times in PBS pH 7.4, the cell suspension was centrifuged for 5 min at 1,000g, and cells were resuspended in the 1:2 mixture of PBS and 100 mM sucrose solution. Cell suspensions were added to seven times higher volume droplets of filtered (0.2 μ m) 1% paraformaldehyde (PFA), 0.15% Triton X-100, 1 mM sodium borate pH 9.2 solution on diagnostic slides, and incubated for 60 min at room temperature. Nuclei were then dried for at least 1 h under the hood. Finally, the slides were washed in 0.4% Photoflo (Kodak) and dried at room temperature. To compare oocyte numbers in adults, we sectioned ovaries of mice (8- μ m-thick sections), identified oocytes by anti-NOBOX (oocyte marker⁶²) immunostaining and counted oocytes in every tenth section. To immunostain spread nuclei and sections, slides were blocked with 2.5% w/v BSA in PBS for 30 min, and then slides were incubated with primary antibodies diluted in blocking solution either for 3 h at room temperature or overnight at 4 °C. Subsequently, slides were washed (3 × 10 min) in PBS and incubated with secondary antibodies at room temperature for 90 min. Finally, slides were washed (3 × 10 min) in PBS and embedded in Slowfade gold antifade mounting media with or without DAPI (Invitrogen). For the quantification of the histone H1T, IHO1 and γ H2AX signal in spread spermatocytes (Supplementary Figs 2 and 6), matched-exposure images were taken and signal intensities were measured with a similar strategy as described earlier⁵. To perform MEI4, REC114 or IHO1 focus quantifications and co-localization experiments, images were analysed using Cell Profiler software⁶³ and customized image analysis pipelines. Given that these proteins apparently formed foci along axes, thresholds were determined empirically to allow the automatic detection of most discernible axis-associated foci. To validate the specificity of co-localization we always compared co-localization in images where the channels of the tested proteins were either unturned or were turned 90° clockwise relative to each other. We considered co-localization significant only if co-localization between foci was significantly reduced after turning one channel 90°. To make sure that the shape of the cell did not influence the results we chose spreads where the nuclei were nearly circular and co-localization was measured only in the largest circular area that could be placed within these cells.

To measure co-localization of MEI4, REC114 or IHO1 foci in wild-type preleptotene spermatocytes, we stained nuclear spreads with guinea pig anti-MEI4, rabbit anti-REC114, and chicken anti-IHO1 antibodies. Preleptotene stage was identified on the basis of the IHO1 staining pattern, which is characteristically punctate at this stage due to the lack of well-developed elongated chromosome axis structures.

Due to the limitation of the nuclear surface spreading method, a variable amount of non-chromatin-bound nuclear content may remain fixed in the nuclear surface spreads. This can give rise to variable punctate background in immunostaining experiments. To reduce the effect of this technical variability and to acquire a more reliable estimate for the number of genuine chromatin-bound MEI4-containing protein assemblies, we co-stained nuclear surface spreads with guinea pig and rabbit anti-MEI4 antibodies. We based our focus counts only on foci that were detected by both antibodies in experiments where we addressed the effect of *Iho1* or *Hormad1* deficiency on MEI4 focus numbers. To validate this approach, we determined what fraction of axis-associated and non-axis-associated MEI4 foci were detected by both guinea pig and rabbit antibodies. 'Background' foci that do not represent genuine chromatin-bound MEI4 complexes are expected to have a random distribution

throughout the nucleus. In contrast, axis-associated foci are expected to represent genuine chromatin-bound MEI4 protein complexes with a higher likelihood. We found that a median of 63% or 34% of guinea pig antibody-detected foci colocalized with rabbit antibody-detected foci on axis or off axis, respectively, in zygotene stage wild-type spermatocytes ($n=30$; Supplementary Table 2, 'wt-gpMEI4-rbMEI4vsAxis'). Similar numbers were obtained for the rabbit antibody stained foci (60% and 37%, respectively). Thus, axis-associated MEI4 foci are more likely to be detected by both antibodies than non-axis-associated foci. These observations are consistent with the idea that MEI4 focus counts that are based on co-staining with guinea pig and rabbit anti-MEI4 antibodies provide a more reliable estimate of the number of chromatin-bound MEI4 protein complexes than focus counts that are based on MEI4 detection with anti-MEI4 antibody from a single species.

Staging of meiotic prophase. Nuclear spreads were staged on the basis of axis development, which was assessed through detection of SYCP3 on meiocyte spreads. Briefly, hazy/punctate SYCP3 staining corresponds to preleptotene, short stretches of axis correspond to leptotene (most axis stretches shorter than 5× the widths of axes), relatively long and incomplete stretches of axes correspond to early zygotene, and complete axes correspond to late-zygotene and pachytene stages (see figure legend of Supplementary Fig. 5). Preleptotene cells are characterized by active DNA replication; therefore, we also used EdU labelling (Supplementary Fig. 1b) in combination with SYCP3 stain to identify preleptotene spermatocytes and to reconfirm the axis morphology that characterizes preleptotene spermatocytes. To identify sub-stages in wild-type pachytene spermatocytes (Supplementary Fig. 2), we used the combination of SYCP3 and either histone H1T⁶⁴ or γ H2AX staining. Pachytene–zygotene transition: all autosomes appear synapsed, but the very ends of autosome axis pairs appear thicker, indicating that synaptonemal complex formation just finished; no H1T staining; γ H2AX-marked chromatin of sex chromosomes is poorly condensed and is often irregular in shape, and γ H2AX is detectable at a low level along synapsed autosomes. Early pachytene: thickness of synapsed axis pairs is largely uniform along their entire length, synapsed PAR region is long (length is >5× the widths) or short (length is <5× but >3× longer than the widths) and no or very weak histone H1T signal. Histone γ H2AX-marked chromatin of sex chromosomes is better condensed with a more regular shape than during zygotene–pachytene transition; γ H2AX is still detectable at low levels along synapsed autosomes. Mid-pachytene: autosomal axis/synaptonemal complex morphology is the same as in early pachytene. Synapsed PAR region is short or very short (length is <3× the widths); histone H1T signal is weak to intermediate strength. We first determined the signal intensity of histone H1T in cells that have very short PAR synapsis, and hence were defined as mid-pachytene. The lowest histone H1T signal from these cells was chosen as a cutoff to distinguish early and mid-pachytene cells in which PAR synapsis was short. Late pachytene: synapsed axes of autosomes are clearly thicker at ends than at interstitial sites. Synapsis at PAR is very short/dot like, or a gap appears between X and Y PAR regions. Histone H1T signal intensity is intermediate to strong. Histone γ H2AX-marked chromatin of sex chromosomes is well condensed; γ H2AX is not detectable along synapsed autosomal axes.

EdU incorporation. Testis cell suspensions were incubated with 10 μ M EdU in DMEM with 10% FCS at 37 °C for 1 h for *in vitro* labelling. EdU incorporation was detected using Alexa Fluor 647 and the Click-iT EdU imaging kit according to the manufacturer's instructions (Invitrogen).

Preparation of protein extracts. To prepare testis extract for IHO1 immunoprecipitation, adult mouse testes were detunicated and macerated by a scalpel in a Petri dish, then resuspended in chromatin extraction buffer (8 mM Tris-HCl pH 7.5, 1% Triton X-100), incubated for 5 min at 4 °C and centrifuged for 10 min at 2,000g. The pellet was resuspended in lysis buffer (50 mM Tris-HCl at pH 7.5, 500 mM NaCl, 1% Triton X-100, 1% NP40, 0.5% sodium deoxycholate, 10 mM MgCl₂) for 60 min at 4 °C. Benzonase (Merck Millipore) was used to digest DNA during lysis. Lysates were sonicated for 5 min with a 400 W Branson sonifier 450 and centrifuged at 20,000g for 10 min. Supernatants were diluted 1:4 with 50 mM Tris-HCl at pH 7.5 and used as input for the immunoprecipitation. To prepare testis extract for MEI4 immunoprecipitation, 12 days postpartum mouse testes were detunicated and macerated by a scalpel in a Petri dish, and then lysed in lysis buffer (50 mM Tris-HCl at pH 7.5, 500 mM NaCl, 1% Triton X-100, 0.5% sodium deoxycholate, 10 mM MgCl₂) for 60 min at 4 °C. Lysates were processed further as described above for IHO1 immunoprecipitation. Preparation of Triton X-100-soluble and -insoluble testis extract fractions was performed as published previously³⁴ (Fig. 1e). All extracts were prepared using protease and phosphatase inhibitors as described earlier³⁴.

Antibody crosslinking, immunoprecipitation and western blotting. Either rabbit anti-IHO1 fragment-1 (3 μ g) antibodies or guinea pig anti-MEI4 (3 μ g) antibodies were crosslinked to 1.5 mg of Dynabeads Protein A (Invitrogen) using 20 mM dimethyl suberimidate according to standard protocols³⁸. After preclearing with

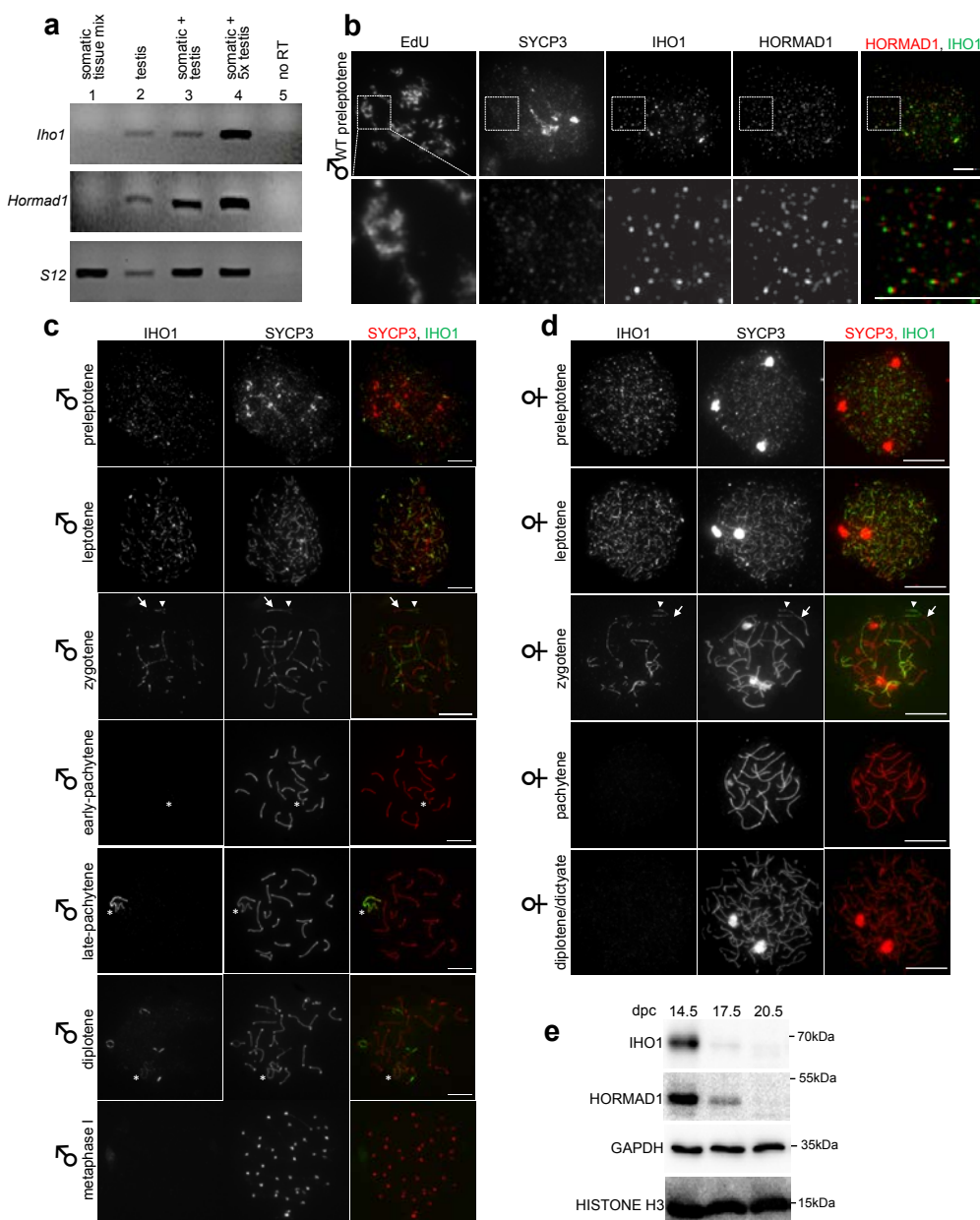
empty protein A beads, protein extracts were incubated with affinity beads overnight at 4 °C. Beads were then washed three times with washing buffer (50 mM Tris-HCl at pH 7.5, 150 mM NaCl, 0.1% Tween20). Immunoprecipitated material was eluted from the beads by incubating the beads in 50 µl Laemmli sample buffer for 10 min at room temperature. The resulting elutions were analysed with SDS-PAGE and immunoblotting using standard methods. Briefly, proteins from extracts were separated on SDS polyacrylamide gels and blotted onto either Nitrocellulose (Hybond ECL Cat. no. RPN2020D, GE Healthcare) (for IHO1 detection in total testis extracts) or PVDF membrane (Cat. no. P2938, Sigma). Membranes were then blocked using BSA 2.5%, 0.05% Tween, TBS blocking solution. To measure levels of SPO11-oligonucleotide complexes in testes, we carried out SPO11 immunoprecipitations and SPO11-oligonucleotide detection as published previously^{12,30}. Both testes from one adult mouse were used for each experiment.

Statistics and reproducibility. R ‘stats’ or ‘exactRanktests’ packages were used to calculate *P* values by one-sample *t*-test, paired *t*-test, Mann–Whitney/Wilcoxon rank sum test exact (non-paired samples) or Wilcoxon signed rank test exact (paired samples). Each conclusion in the manuscript was based on results that were reproduced in at least two independent experiments and at least two mice of each genotype.

Data availability. Supplementary Table 2 contains statistics source data for Figs 2, 3 and 5–8 and Supplementary Figs 2 and 5–7 and for anti-MEI4 antibody validation and MEI4 foci axis association (sheets ‘gpMEI4-rbMEI4-coloc’, ‘gp&rb MEI4 WTvsMEI4ko’ and ‘wt-gpMEI4-rbMEI4vsAxis’). All other data supporting the findings of this study are available from the corresponding author on request.

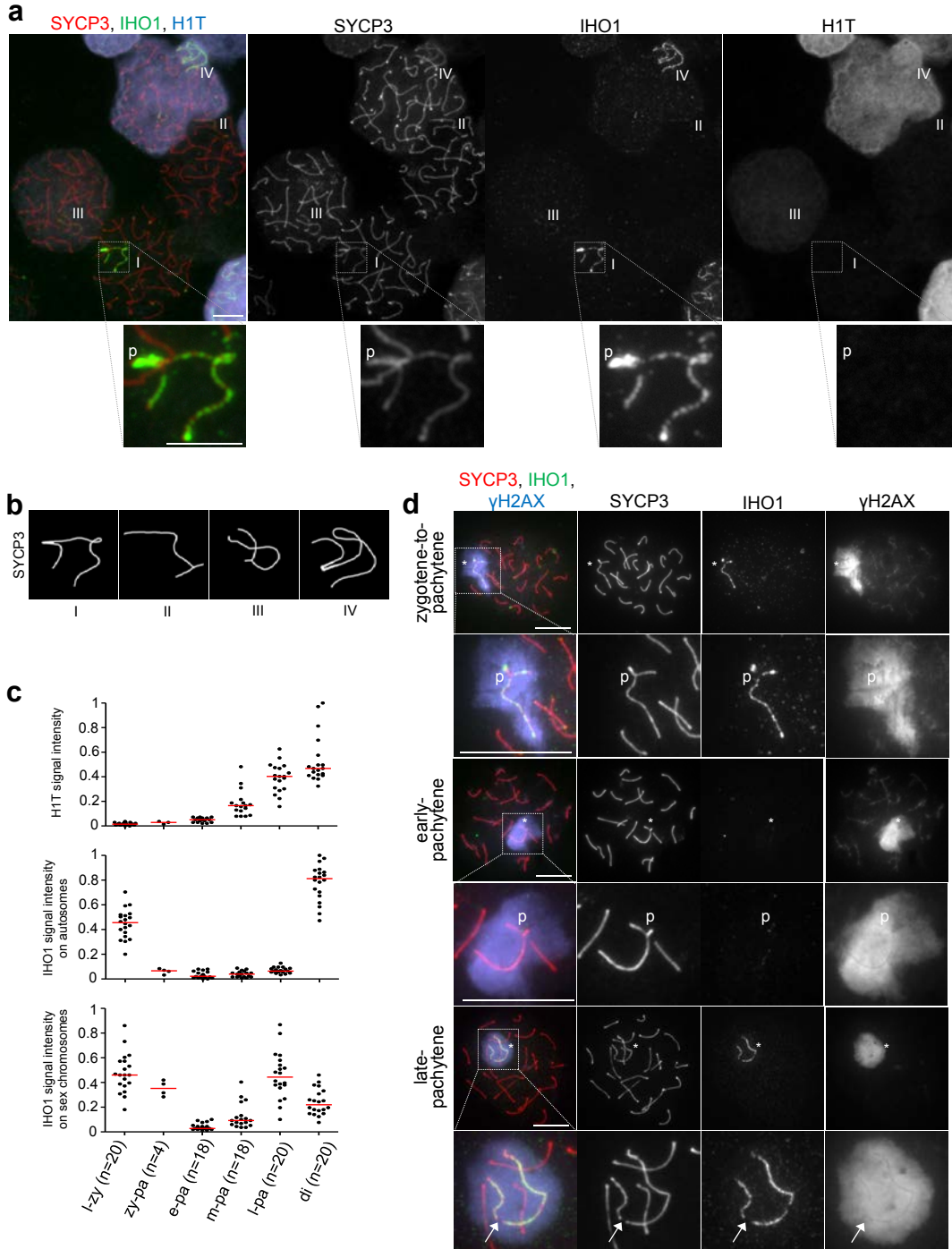
- 50. Koegl, M. & Uetz, P. Improving yeast two-hybrid screening systems. *Brief. Funct. Genomic. Proteomic.* **6**, 302–312 (2007).
- 51. Gietz, R. D., Triggs-Raine, B., Robbins, A., Graham, K. C. & Woods, R. A. Identification of proteins that interact with a protein of interest: applications of the yeast two-hybrid system. *Mol. Cell. Biochem.* **172**, 67–79 (1997).

- 52. Kaiser, C., Michaelis, S. & Mitchell, A. *Methods in Yeast Genetics, a Cold Spring Harbor Laboratory Manual* (Cold Spring Harbor Laboratory Press, 1994).
- 53. Wojtasz, L., Daniel, K. & Toth, A. Fluorescence activated cell sorting of live female germ cells and somatic cells of the mouse fetal gonad based on forward and side scattering. *Cytometry A* **75A**, 547–553 (2009).
- 54. Testa, G. *et al.* A reliable lacZ expression reporter cassette for multipurpose, knockout-first alleles. *Genesis* **38**, 151–158 (2004).
- 55. Kranz, A. *et al.* An improved Flp deleter mouse in C57Bl/6 based on Flpo recombinase. *Genesis* **48**, 512–520 (2010).
- 56. Lallemand, Y., Luria, V., Haffner-Krausz, R. & Lonai, P. Maternally expressed PGK-Cre transgene as a tool for early and uniform activation of the Cre site-specific recombinase. *Transgenic Res.* **7**, 105–112 (1998).
- 57. Baudat, F., Manova, K., Yuen, J. P., Jasir, M. & Keeney, S. Chromosome synapsis defects and sexually dimorphic meiotic progression in mice lacking Spo11. *Mol. Cell* **6**, 989–998 (2000).
- 58. Halow, E. & Lane, D. *Using Antibodies: A Laboratory Manual* (Cold Spring Harbor Laboratory Press, 1999).
- 59. Shibuya, H., Morimoto, A. & Watanabe, Y. The dissection of meiotic chromosome movement in mice using an *in vivo* electroporation technique. *PLoS Genet.* **10**, e1004821 (2014).
- 60. Shoji, M., Chuma, S., Yoshida, K., Morita, T. & Nakatsuji, N. RNA interference during spermatogenesis in mice. *Dev. Biol.* **282**, 524–534 (2005).
- 61. Peters, A. H., Plug, A. W., van Vugt, M. J. & de Boer, P. A drying-down technique for the spreading of mammalian meiocytes from the male and female germline. *Chromosome Res.* **5**, 66–68 (1997).
- 62. Suzumori, N., Yan, C., Matzuk, M. M. & Rajkovic, A. Nobox is a homeobox-encoding gene preferentially expressed in primordial and growing oocytes. *Mech. Dev.* **111**, 137–141 (2002).
- 63. Kamentsky, L. *et al.* Improved structure, function and compatibility for CellProfiler: modular high-throughput image analysis software. *Bioinformatics* **27**, 1179–1180 (2011).
- 64. Inselman, A., Eaker, S. & Handel, M. A. Temporal expression of cell cycle-related proteins during spermatogenesis: establishing a timeline for onset of the meiotic divisions. *Cytogenet. Genome Res.* **103**, 277–284 (2003).



Supplementary Figure 1 IHO1 expression and localization in wild-type spermatocytes. (a) RT-PCR was used to test expression of *Iho1*, a meiosis marker (*Hormad1*) and a “house-keeping” gene (*S12*) in testis and a somatic tissue mix. cDNAs were prepared from four RNA mixtures: (1) somatic tissue mix: 1 µg of RNA mix of 59 ng total RNAs from 17 somatic tissues (see Materials and Methods for the tissue list). (2) testis: 59 ng total testis RNAs from adult. (3) somatic+testis: 1 µg of RNA mix of 59 ng total testis RNAs and 941 ng of somatic tissue mix. (4) somatic+5xtestis: 1 µg of RNA mix of 295 ng total testis RNAs and 705 ng of somatic tissue mix. (5) no RT: no RT control with somatic+5xtestis. *Iho1* specific PCR-products were amplified only from templates that contain testis cDNA. (b) Testis cell suspensions were incubated in the presence of EdU to label cells with ongoing DNA replication. An EdU-labelled preleptotene cell is shown, where SYCP3, IHO1 and HORMAD1 were detected by immunofluorescence. HORMAD1 and IHO1 form foci that often colocalize. The red channel is

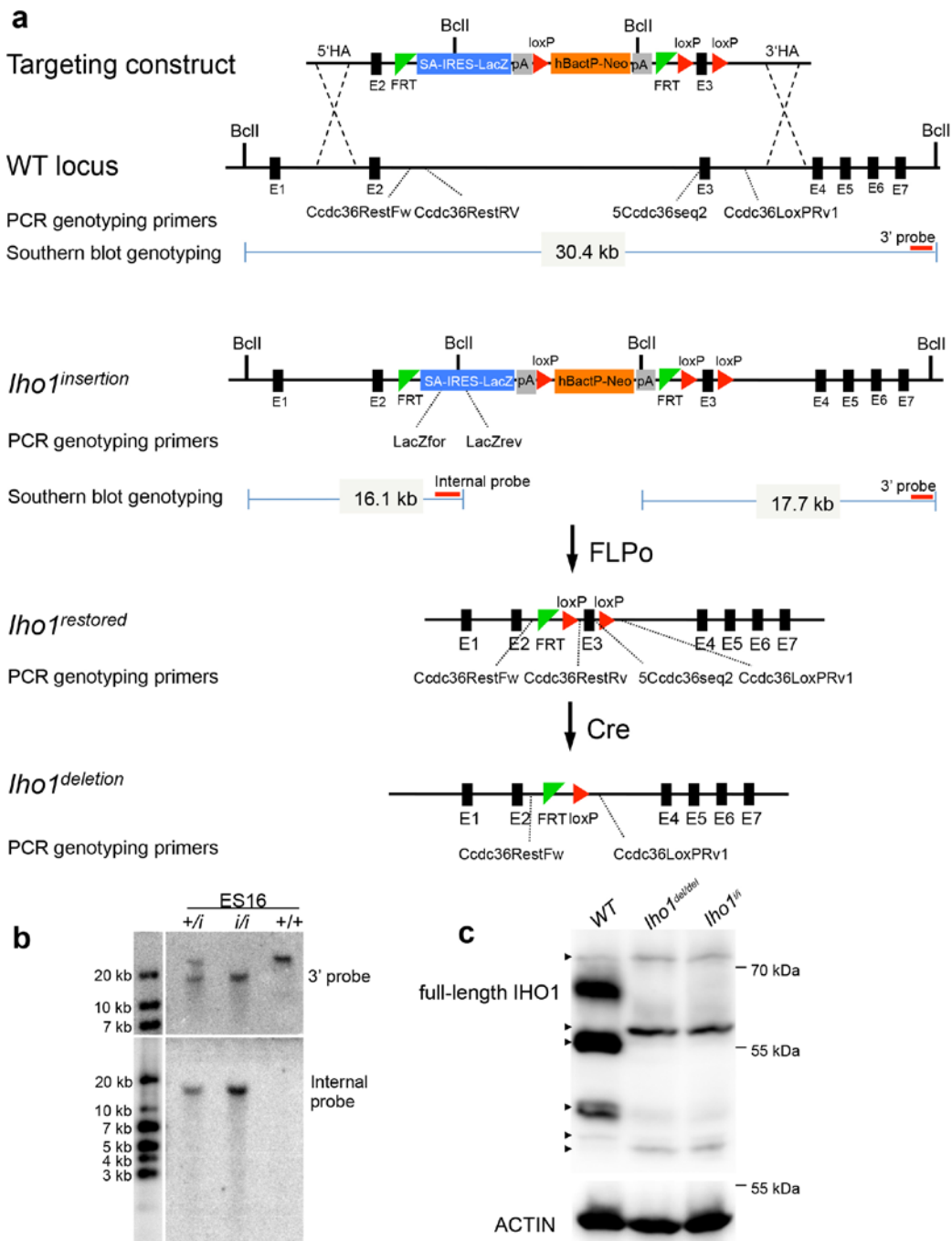
shifted three pixels to the right to allow better visualization of colocalizing signals in the enlarged inset of the overlay image. (c, d) SYCP3 and IHO1 were detected on nuclear surface spreads of wild-type spermatocytes (c) and oocytes (d) at the indicated stages. Oocytes were collected from ovaries either at 14.5 (preleptotene, leptotene and zygotene) or 20.5 (pachytene, diplotene) days post coitum (dpc). Arrow and arrowhead mark synapsed and unsynapsed axes in zygotene cells, respectively. Asterisks (c) mark the largely non-homologous X and Y chromosomes, which synapse only in their short homologous PAR regions in spermatocytes. Note that IHO1 is depleted from X and Y chromosomes in early-pachytene, but it reappears on them in late-pachytene spermatocytes. Scale bars, 10 µm. (e) Indicated proteins were detected in protein extracts from 14.5, 17.5 and 20.5 dpc ovaries, which are rich in leptotene-to-zygotene, pachytene and diplotene-dictyate oocytes, respectively. Histone H3 and GAPDH are loading controls. See Supplementary Fig. S8 for unprocessed gel-scans.



Supplementary Figure 2 IHO1 localization from late-zygotene to diplotene. **(a, d)** SYCP3, IHO1 and histone H1T variant (marker of mid-pachytene onwards, a) or γ H2AX (d) were detected by immunofluorescence on nuclear surface spreads of wild-type spermatocytes. The images show high levels of IHO1 on sex chromosome axes at the zygotene-to-pachytene transition (a: I; d) and late-pachytene (a: IV; d) while IHO1 levels are much lower in early- (a: II, d) and mid-pachytene (a: III). (d) Asterisk marks sex chromosomes. (a, d) Enlarged insets show higher magnification images of sex chromosomes. P marks the PAR region, where IHO1 is detectable during the zygotene-to-pachytene transition. Arrow in d points at the gap between X and Y PAR regions during late-pachytene. Scale bars, 10 μ m. **(b)** Drawings of sex chromosome axes

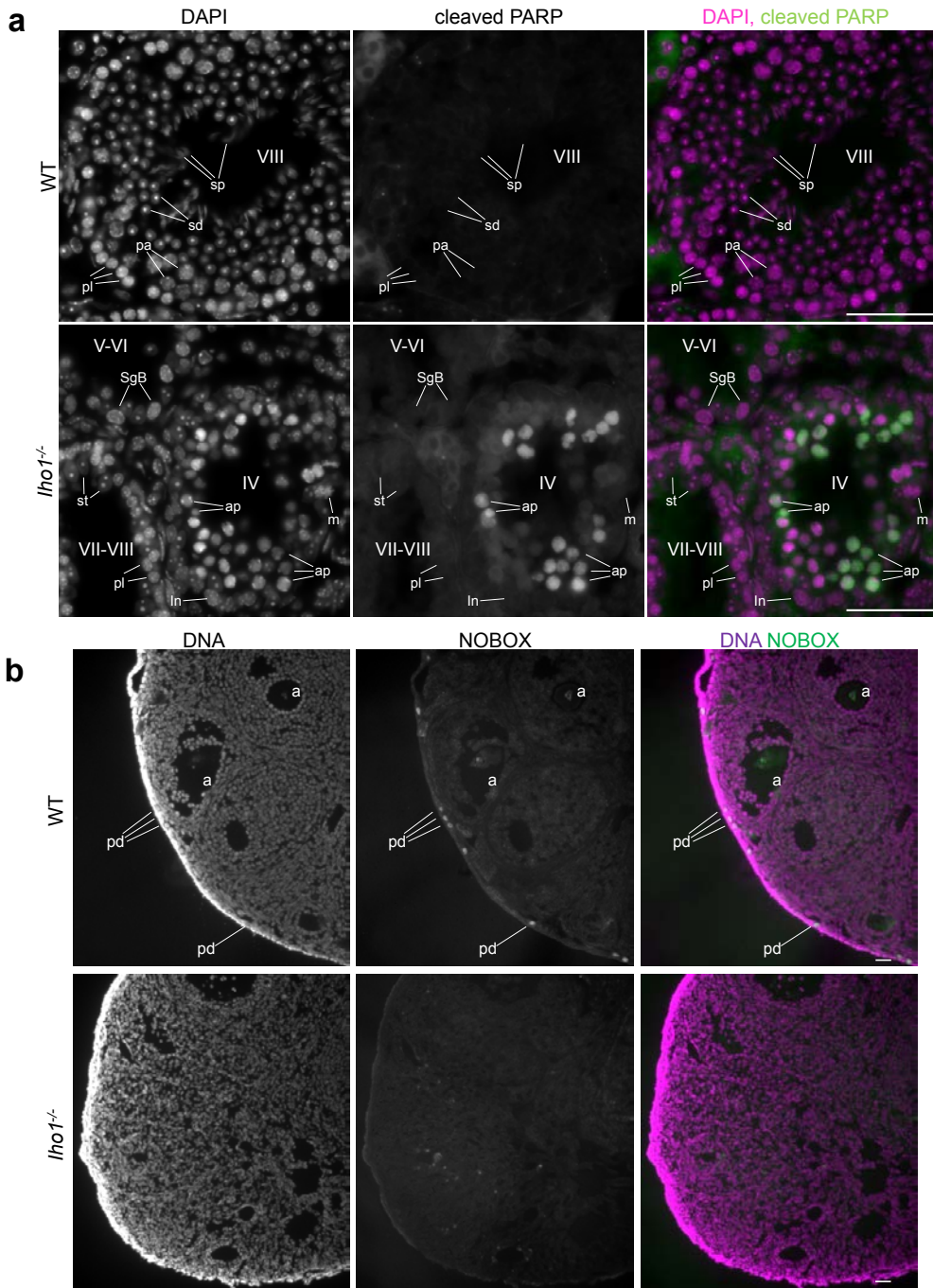
in the four marked cells of a. **(c)** Quantification of H1T signal on chromatin (upper panel), and IHO1 signal on autosomal axes (middle panel, measured on unsynapsed axes in zygotene and diplotene, measured on synapsed axes in other stages) and unsynapsed sex chromosomal (lower panel) axes during late-zygotene (I-zy), zygotene-to-pachytene transition (zy-pa), early-pachytene (e-pa), mid-pachytene (m-pa), late-pachytene (I-pa) and diplotene (di). Median values are shown by red horizontal bars. Numbers of nuclei analyzed are indicated (n). Quantification is shown from a single experiment, the conclusions of which were reconfirmed in further four experiments without *in silico* quantification of protein-signal intensities in images. Primary source data of graphs are shown in Supplementary Table 2.

SUPPLEMENTARY INFORMATION



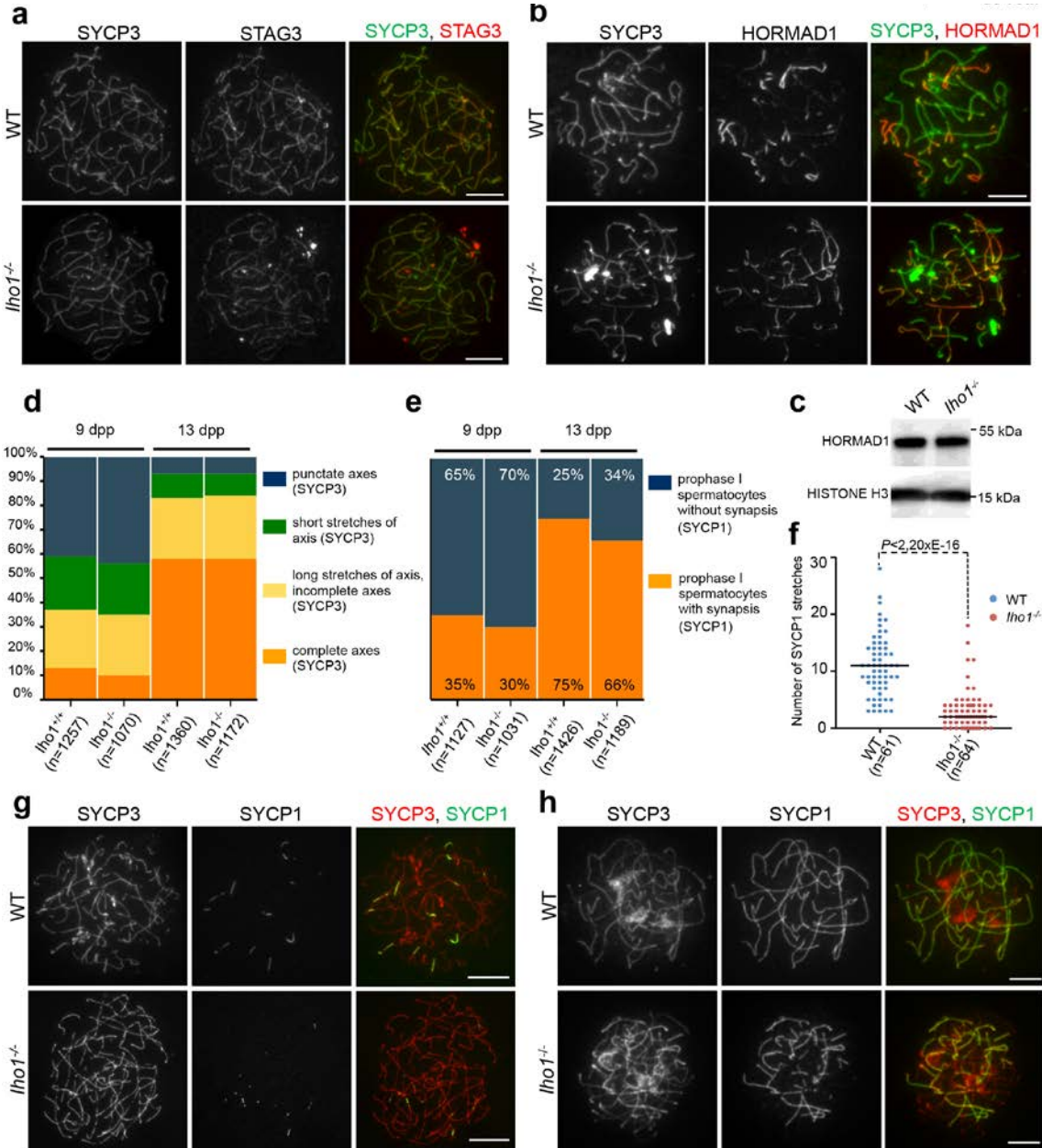
Supplementary Figure 3 *Iho1* targeting strategy. (a) Schematics of the targeting construct, the wild-type (WT) and modified *Iho1* genomic locus. Black boxes represent exons (not to scale). Recombination at the homology arms (HA) of the targeting construct modifies intron 2 by introducing: 1) an additional exon (SA-IRES-LacZ) that contains a strong splice acceptor site (SA) and poly-adenylation site (left grey box), 2) a transcriptional unit that contains the strong housekeeping human β-Actin promoter (*BactP*) driving the neomycin (Neo) resistance gene as a selection marker. This modification of intron 2 disrupts the *Iho1* open reading frame after the 80th codon (*Iho1^{insertion}* allele). Recombination catalyzed by FLPO at FRT sites removes the SA-IRES-LacZ exon and the BactP-Neo gene, and restores the IHO1 ORF (*Iho1^{restored}*). *Iho1^{restored}* is a functional allele that can be disrupted by Cre-mediated recombination between loxP sites (*Iho1^{deletion}*). Excision of exon 3 causes a frameshift after the 80th codon. The positions of PCR-genotyping primers are indicated. Red bars mark the 3' and the internal Southern blot

probes; the predicted length of restriction fragments is indicated. (b) Southern blot of DNA from wild-type (+/+), *Iho1^{+/+insertion}* (+/-), *Iho1^{insertion/insertion}* (-/-) mice derived from the targeted embryonic stem cell clones (ES16). DNA was digested with BclI (both upper and lower panel). The blots indicate a single integration of the targeting cassette in the *Iho1* locus. (c) Western blot analysis of extracts prepared from testes of wild-type (WT), *Iho1^{deletion/deletion}* (*Iho1^{del/del}*) and *Iho1^{insertion/insertion}* (*Iho1^{fl/fl}*) mice. Rabbit antibody against the first 144 amino acid of IHO1 did not detect full length IHO1 protein in *Iho1^{deletion/deletion}* (*del/del*), *Iho1^{insertion/insertion}* (*fl/fl*) testes (upper panel). Actin was used as a loading control (lower panel). Arrowheads mark bands that were not detected reproducibly under distinct blotting and blocking conditions. Hence, these bands are considered non-specific. The pattern of these non-specific bands is distinct in testis extracts of adult wild-type and *Iho1*-deficient mice, which is likely caused by severely altered cellularity in the testis of *Iho1*-deficient mice. Unprocessed gel-scans are shown in Supplementary Fig. S8.



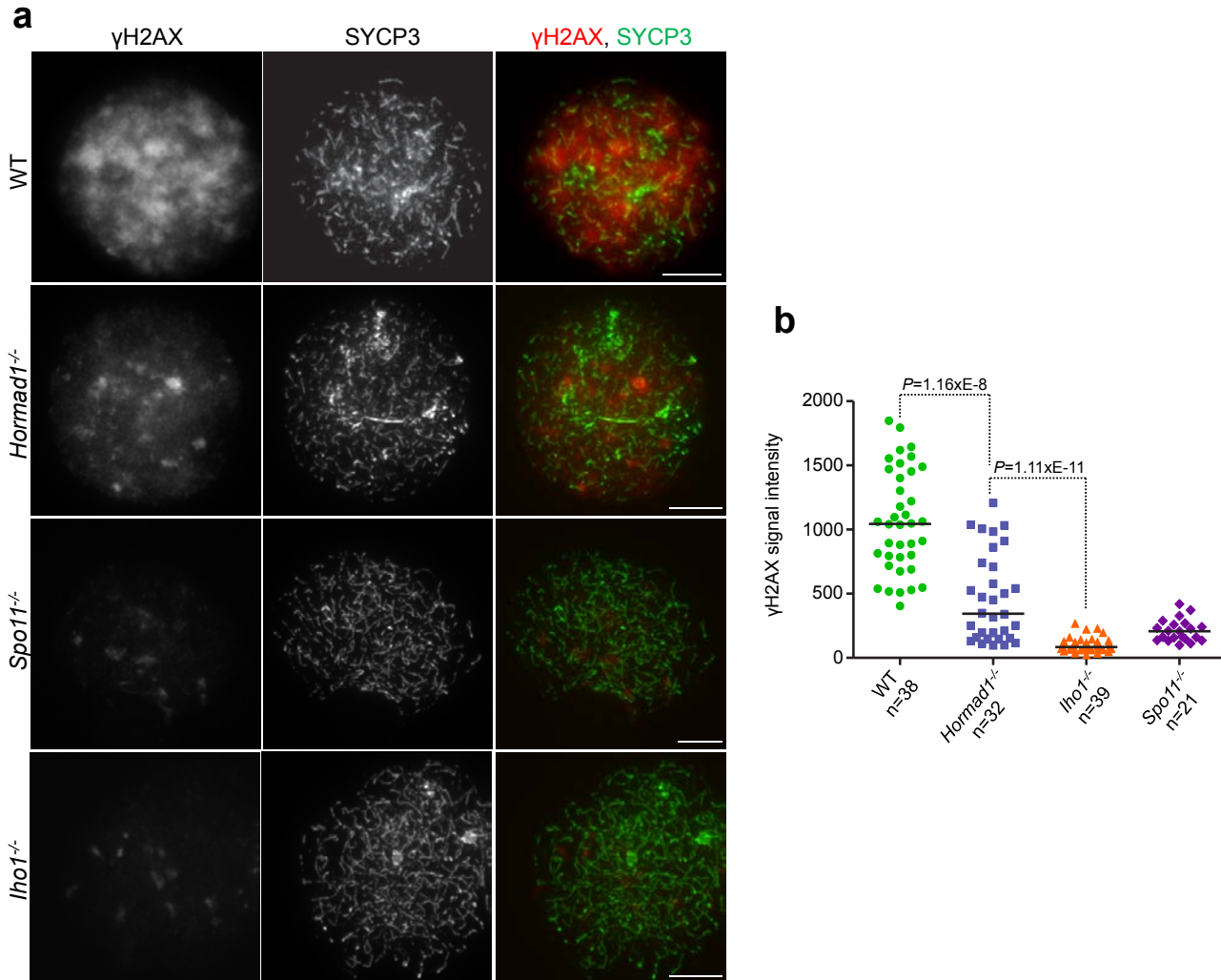
Supplementary Figure 4 *Iho1*^{-/-} mice are deficient in germ cells from late meiotic prophase onwards in both sexes. (a) Cryosections of testes from 16-week-old wild-type (WT) and *Iho1*^{-/-} mice. DNA was detected by DAPI, apoptotic cells were detected by nuclear cleaved PARP1 immunostaining. (upper panel) We show a stage VIII wild-type testis tubule, which contains several layers of germ cells at distinct spermatogenic stages: preleptotene (pl) and late-pachytene (pa) spermatocytes and post-meiotic spermatids (sd) and spermatozoa (sp). (lower panel) *Iho1*^{-/-} meiocytes underwent apoptosis at a stage corresponding to wild-type mid-pachytene in stage IV tubules. Consequently, spermatocytes were not found in the inner layers of testis tubules beyond stage IV, and post-meiotic spermatids and spermatozoa were also missing from *Iho1*^{-/-} testes. To illustrate this, stage IV, V-VI and VII-VIII tubules of *Iho1*^{-/-} mice are shown. Apoptotic spermatocytes (ap) are detected

in the stage IV tubule, which was identified by the presence of mitotic intermediate spermatogonia (m) and intermediate spermatogonia (In). Stage V-VI and VII-VIII tubules contain somatic Sertoli cells (st) and spermatogonia B (SgB) or preleptotene (pl) spermatocytes, respectively, but more advanced spermatogenic cells are missing. (b) Nobox (oocyte marker) was detected by immunofluorescence on cryosections of ovaries from 6-week-old mice. DNA was stained by DAPI. Oocytes in primordial (pd) and antral (a) follicles are shown in the section of a wild-type ovary. In contrast, oocytes are not detected in the shown *Iho1*^{-/-} ovary section. Quantification of oocytes revealed much fewer oocytes in *Iho1*^{-/-} than in wild-type ovaries at 6 weeks of age. Oocytes were counted on every tenth section of ovaries: a total of 624 and 724 oocytes in one ovary from each of two wild-type mice, and 3, 4, 2 and 9 oocytes in one ovary of each of four *Iho1*^{-/-} mice. Scale bars, 50μm.



Supplementary Figure 5 Synaptonemal complex formation, but not axis formation, is defective in *Iho1*^{-/-} mice. **(a, b)** SYCP3 and either STAG3 cohesin (**a**) or HORMAD1 (**b**) were detected on nuclear spreads of wild-type (WT) and *Iho1*^{-/-} spermatocytes. Axis morphology, axis association of STAG3 and enrichment of HORMAD1 on unsynapsied axes are similar in wild type and *Iho1*^{-/-}. **(b)** The same *Iho1*^{-/-} spermatocyte is shown in Fig. 2b. Scale bars, 10 μm. **(c)** Indicated proteins were detected in extracts of wild-type and *Iho1*^{-/-} testes. See Supplementary Fig. S8 for unprocessed gel-scans. **(d-f)** Axis and synaptonemal complex development were assessed by detecting SYCP3 (axis) and SYCP1 (synaptonemal complex) in nuclear spreads of spermatocytes from litter-mate pairs of wild-type and *Iho1*^{-/-} mice. Ages of mice are indicated in **d** and **e** (days postpartum-dpp). Results of two (**d**) or three (**e**) experiments were pooled; counted cell numbers are indicated (*n*); source data are available in Supplementary Table 2. **(d)** Fractions of spermatocytes belonging to four different axis-development category are shown: (blue) punctate axes, preleptotene; (green) short stretches of axis, leptotene;

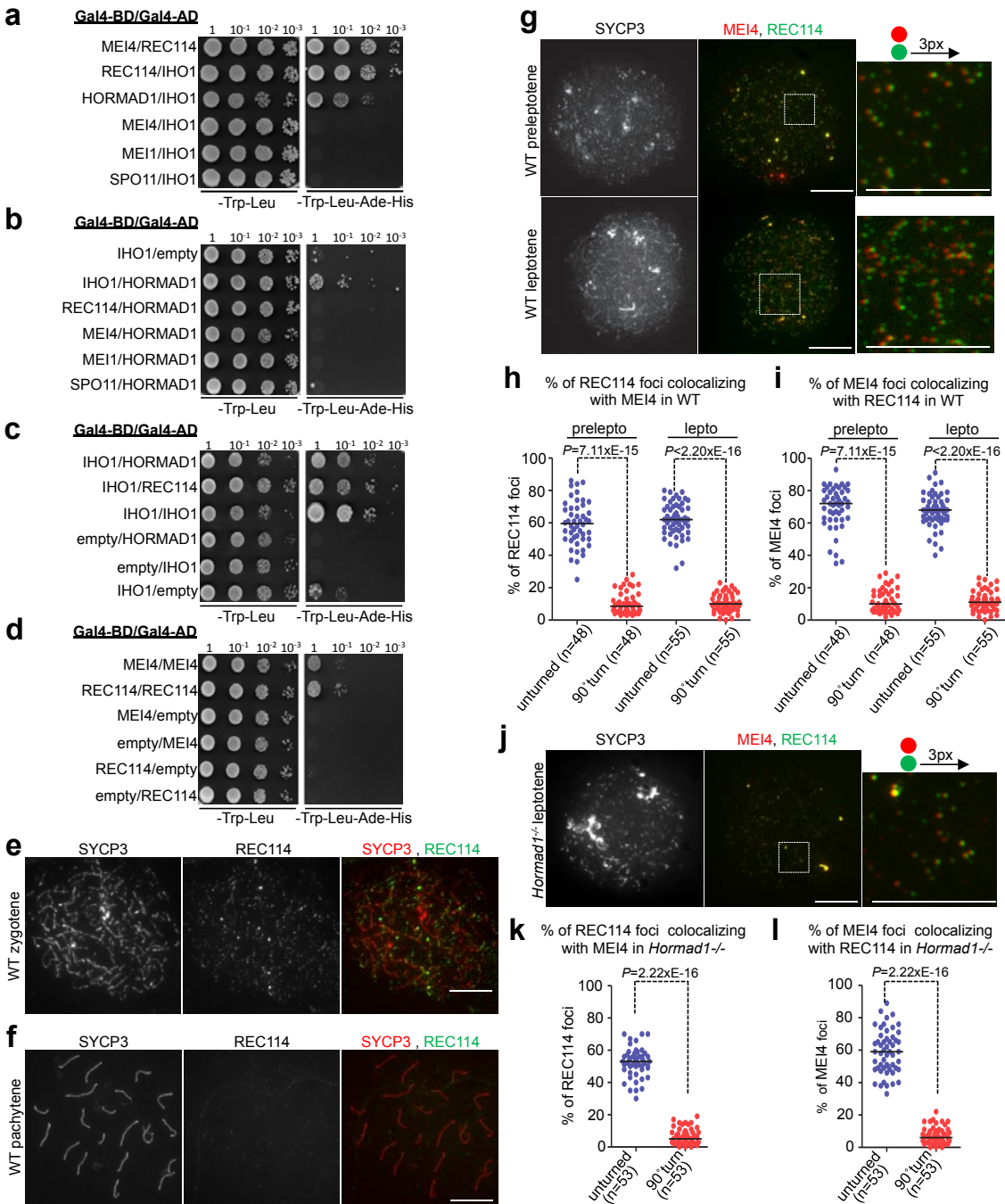
(yellow) relatively long but incomplete axes, early-zygotene; (orange) fully formed axes, late-zygotene and pachytene. Axis development did not differ significantly in *Iho1*^{-/-} and wild type. **(e)** shows fractions of spermatocytes with either (blue) no synaptonemal complex, or (orange) variable levels of synapsis ranging from short synaptonemal complex stretches to complete autosomal synaptonemal complex (the latter is observed only in wild type). Fractions of spermatocytes with synaptonemal complex is significantly lower in *Iho1*^{-/-} than in wild-type mice at 13dpp ($p=0.245$ at 9dpp, $p=0.039$ at 13dpp, paired t-test). **(f)** Numbers of SYCP1 stretches are shown in early-zygotene wild-type and *Iho1*^{-/-} spermatocytes at 13dpp. The median number (bars) of SYCP1 stretches is 5.5-fold lower in *Iho1*^{-/-} than in wild type (Mann-Whitney test). Thus, synapsis initiation appears less efficient in *Iho1*^{-/-} than in wild type. **(g, h)** SYCP3 and SYCP1 were detected on nuclear spreads of wild-type and *Iho1*^{-/-} spermatocytes (**g**, early-zygotene) or oocytes (**h**, 14.5dpc littermate fetuses). *Iho1*^{-/-} oocytes display similar synaptonemal complex formation defects as *Iho1*^{-/-} spermatocytes (Fig. 2).



Supplementary Figure 6 IHO1 is required for the accumulation of γ H2AX on the chromatin of leptotene and early-zygote spermatocytes. **(a)** SYCP3 (chromosome axis) and γ H2AX were detected by immunofluorescence in nuclear spreads of leptotene and early-zygote wild-type (WT), *Hormad1*^{-/-}, *Iho1*^{-/-} and *Spo11*^{-/-} spermatocytes. Matched exposure images of γ H2AX are shown. Bars, 10 μ m. **(b)** Quantification of total nuclear γ H2AX immunofluorescence signal in nuclear spreads of wild-type (WT), *Hormad1*^{-/-}, *Spo11*^{-/-} and *Iho1*^{-/-} leptotene and early-zygote spermatocytes. Arbitrary units are shown. Median γ H2AX intensities are marked, and n shows analyzed spermatocyte number. Combined results from three (wild type and *Iho1*^{-/-}) or two (*Hormad1*^{-/-} and *Spo11*^{-/-}) experiments are shown. Primary

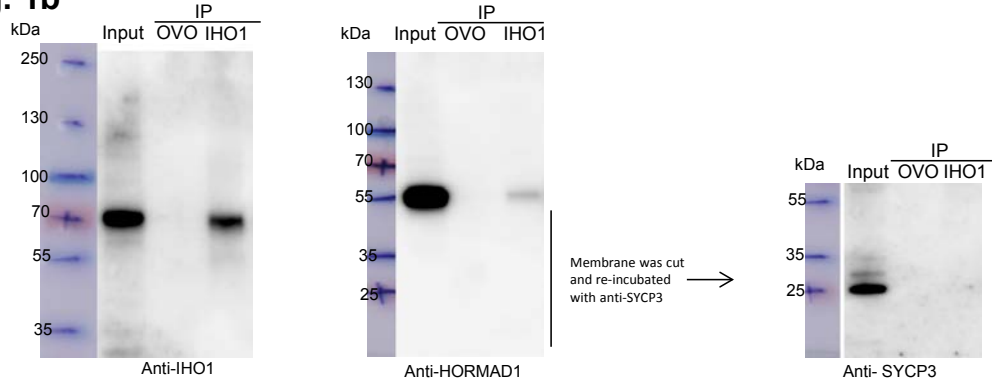
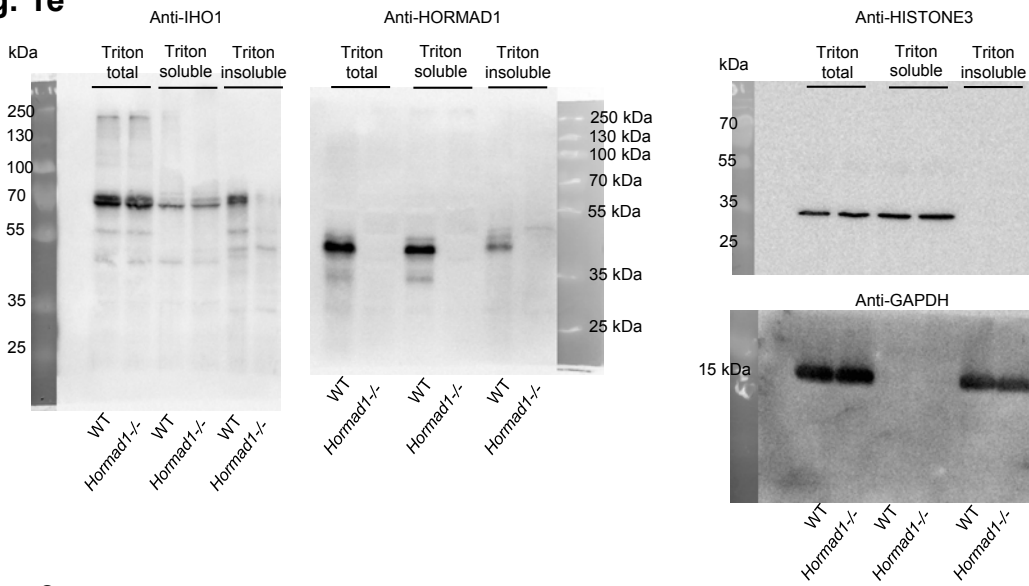
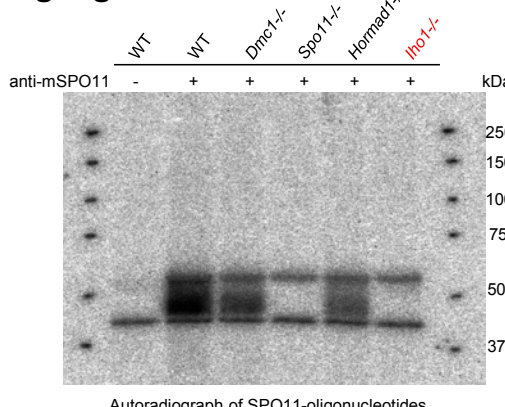
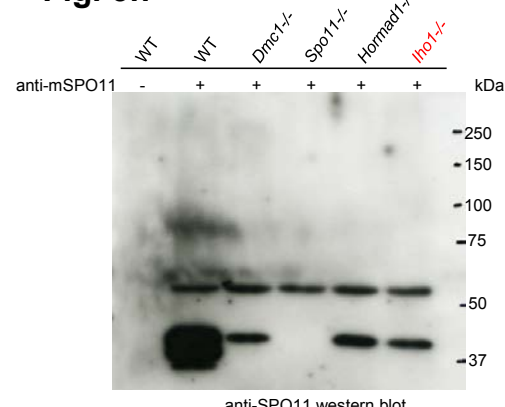
source data of graphs are available in Supplementary Table 2. The γ H2AX-specific signal is significantly lower in *Iho1*^{-/-} than in wild-type (14-fold) and *Hormad1*^{-/-} (4.6-fold) spermatocytes, and it is not higher than the signal in *Spo11*^{-/-} spermatocytes, which are completely deficient in programmed DSB formation (Mann-Whitney test). This indicates that DSB formation is similarly defective in *Spo11*^{-/-} and *Iho1*^{-/-} spermatocytes, and more defective than in *Hormad1*^{-/-} spermatocytes. Note that leptotene and early-zygote cells are not homogenous populations with respect to DSB numbers in DSB formation-proficient backgrounds, because DSBs are actively introduced into the genome during these stages. Variation in γ H2AX levels of wild-type and *Hormad1*^{-/-} spermatocytes probably reflects this heterogeneity.

SUPPLEMENTARY INFORMATION



Supplementary Figure 7 REC114 interacts with IHO1 and forms co-foci with MEI4 on chromatin in spermatocytes. **(a-d)** Yeast two-hybrid assays testing interactions of indicated proteins. 10 µl of yeast cell suspensions of indicated optical densities were plated onto indicated dropout plates. **(a)** The MEI4-REC114 interaction served as a positive control. **(b)** The single colony in the SPO11/HORMAD1 lane of the -Trp-Leu-Ade-His plate was not reproducible, hence we do not consider it as a sign of true interaction. **(b-c)** The IHO1 bait weakly self-activated (first and last rows in **b** and **c**, respectively). Nevertheless, enhanced growth of experimental yeast strains in comparison to controls indicates IHO1-IHO1 interaction, and provided a reciprocal reconfirmation of REC114-IHO1, and HORMAD1-IHO1 interactions from **a**. **(e, f, g, j)** Indicated proteins were detected by immunofluorescence in nuclear spreads of wild-type (WT) and *Hormad1*^{-/-} spermatocytes at indicated stages. Scale bars, 10µm. REC114 foci are present along chromosome axes in zygotene (**e**), but essentially absent

in pachytene (**f**). **(g, j)** Frequent colocalization of REC114 and MEI4 foci was observed in wild-type (**g**) and *Hormad1*^{-/-} (**j**) spermatocytes. The green channel is shifted three pixels to the right in the enlarged insets to allow better visualization of colocalization. **(h, i, k, l)** Quantification of colocalization between REC114 and MEI4 in wild-type preleptotene and leptotene (**h, i**), or *Hormad1*^{-/-} (**k, l**) leptotene spermatocytes. Data points show fractions of REC114 foci that colocalize with MEI4 (**h, k**), and fractions of MEI4 foci that colocalize with REC114 (**i, l**). Medians are marked, and numbers of analyzed cells are indicated (n); results from two independent experiments were pooled; source data of graphs are shown in Supplementary Table 2. To control for random overlap between foci of examined proteins, colocalization frequencies were measured with (red, 90° turn) and without (blue, unturned) rotating the images of MEI4 and REC114 by 90° relative to each other. Significantly lower (Mann-Whitney test) colocalization frequencies were found after rotation in all cases.

Fig. 1b**Fig. 1e****Fig. 3g****Fig. 3h**

Supplementary Figure 8 Unprocessed scans of full blots and gels of indicated figures.

Fig. 6c

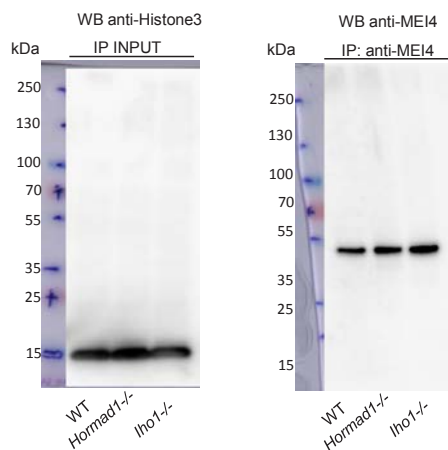


Fig. 8d

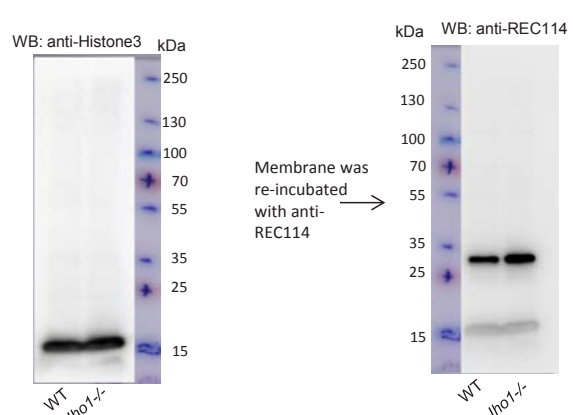


Fig. S1e

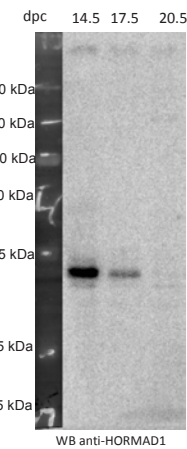
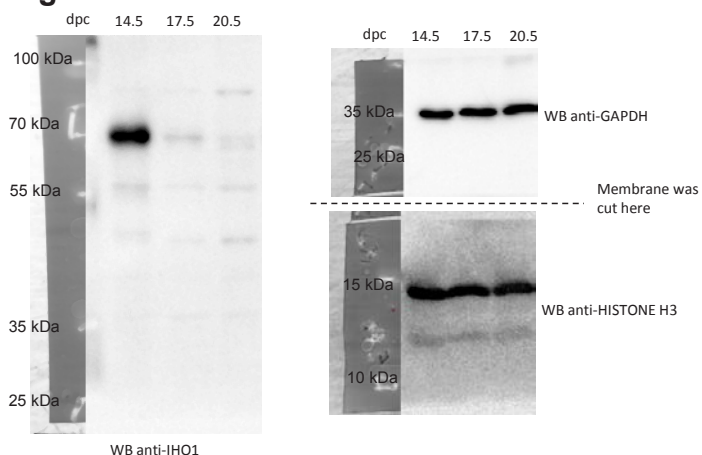


Fig. S5c

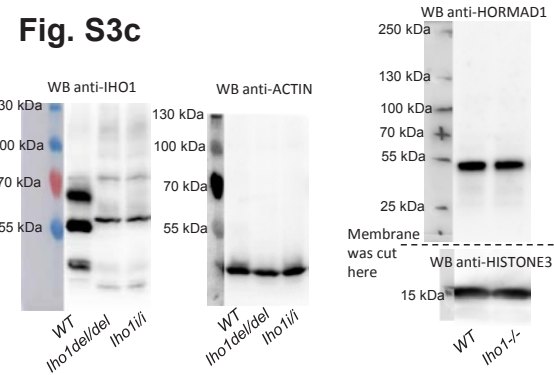


Fig. S3b

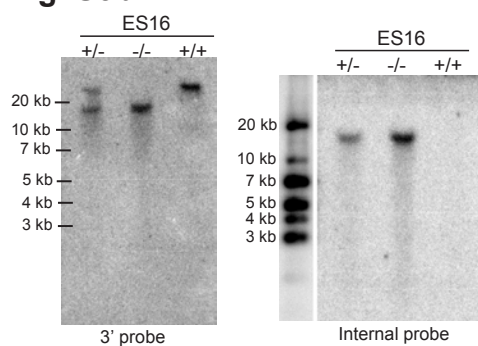


Fig. S3c

Supplementary Figure 8 continued

Supplementary Figure Legends

Supplementary Table 1 HORMAD1 yeast two-hybrid screen results.

Supplementary Table 2 Source data of main and supplementary figures. Source data for Fig. 2, 3, 5, 6, 7, 8, Supplementary Fig. S2, S5, S6 and S7 are provided in the corresponding data sheets. Sheets called “gpMEI4 rbMEI4 coloc”, “gp&rb MEI4 WTvsMEI4ko” and “wt-gpMEI4-rbMEI4vsAxis” contain data that is relevant to anti-MEI4 antibody validation and MEI4 foci axis association measurement.